Journal of Environmental Chemical Engineering 14 (2026) 122337

Contents lists available at ScienceDirect

Journal of Environmental Chemical Engineering

journal homepage: www.elsevier.com/locate/jece

Double network hydrogel–biochar composites with enhanced water absorption and salinity tolerance for sustainable agriculture

Dzureen Julaihi [a], Cindy Soo Yun Tan [a,*], Lin-Chi Wang [b], Mohamad Izzat Arif Nordin [a], Kavirajaa Pandian Sambasevam [c], Suk-Fun Chin [d], Fui Kiew Liew [a], Su Shiung Lam [e,f], Peter Nai Yuh Yek [g], Margaret Abat [h], Nazrizawati Ahmad Tajuddin [i]

[a] Faculty of Applied Sciences, Universiti Teknologi MARA, Kota Samarahan, Sarawak 94300, Malaysia
[b] Department of Marine Environmental Engineering, National Kaohsiung University of Science and Technology, 142, Haijhuan Road, Nanzih District, Kaohsiung 81157, Taiwan
[c] Advanced Materials for Environmental Remediation (AMER), Faculty of Applied Sciences, Universiti Teknologi MARA, Cawangan Negeri Sembilan, Kampus Kuala Pilah, Kuala Pilah, Negeri Sembilan 72000, Malaysia
[d] Faculty of Resource Science and Technology, Universiti Malaysia Sarawak, Kota Samarahan, Sarawak 94300, Malaysia
[e] Higher Institution Centre of Excellence (HICoE), Institute of Tropical Aquaculture and Fisheries (AKUATROP), Universiti Malaysia Terengganu, Kuala Nerus, Terengganu 21030, Malaysia
[f] University Centre for Research and Development, Department of Chemistry, Chandigarh University, Gharuan, Mohali, Punjab, India
[g] Centre for Research of Innovation and Sustainable Development, University of Technology Sarawak, No.1, Jalan Universiti, Sibu, Sarawak 96000, Malaysia
[h] Agriculture Research Centre Semongok, Department of Agriculture Sarawak, KM20, Borneo Heights Road, Kuching, Sarawak 93250, Malaysia
[i] School of Chemistry & Environment, Faculty of Applied Sciences, Universiti Teknologi MARA, Shah Alam, Selangor 40450, Malaysia

ARTICLE INFO

Keywords:
Hydrogel-biochar composites
Response surface methodology-central composite design optimization
Water absorbency
Salinity tolerance
Cyclic stability
Water retention agent

ABSTRACT

Inefficient irrigation practices in conventional irrigated agriculture contribute significantly to water scarcity, resource wastage and declining soil health. Coupled with accelerating climate change and urbanization, these challenges highlight the urgent need for innovative water retention agents (WRAs) that can boost water absorbency and promote water-use efficiency for sustainable agriculture. Novel double network hydrogel-biochar composites (DNHBCS*x*) were synthesized by employing a facile one-pot method, integrating covalently-crosslinked potassium poly(acrylate-*co*-acrylamide) (P(AA-*co*-AM)), dynamically-crosslinked poly(vinyl alcohol) (PVA) and palm kernel shell biochar (BC). Three key reactants, namely methylene bisacrylamide crosslinker (MBA), PVA and BC loadings, were optimized for equilibrium water absorption (EW) using Response Surface Methodology-Central Composite Design (RSM-CCD) under deionized (DI) water and saline (0.9% w/v NaCl) conditions. The ANOVA confirmed the relevance of the quadratic polynomial model ($p < 0.05$), revealing PVA, BC and MBA-PVA interaction as dominant factors affecting EW. The optimized formulation, DNHBCS6 exhibited EW of 321.46 g/g in DI water, 34.59 g/g in 0.9% w/v NaCl and 40.94 g/g in 0.9% w/v KCl. The BC-reinforced double network structure imparted controlled swelling behaviour, pH responsiveness, salt-responsive reversible swelling and resistance to cyclic structural fatigue while retaining high water absorbency (EW $\geq$220 g/g). Soil application tests showed increased water holding capacity in sandy loam from 81.47% to 121.47% and retained 29.33% moisture by DNHBCS6 after 21 days, confirming its effectiveness in coarse-textured soils. Achieving a balanced synergy of EW, structural durability and saline tolerance, DNHBCS6 emerges as a robust WRA for agricultural water-use efficiency, particularly in drought-prone and saline-affected regions.

1. Introduction

Irrigated agriculture plays a critical role in ensuring food security to meet increasing food demand, but conventional practices are often associated with excessive chemical fertilization and inefficient conventional irrigation methods which exhibit high nutrient and water losses via surface runoff, evaporation and uneven distribution, leading to significant resource wastage, reduced resource sustainability and

* Corresponding author.
E-mail address: cindytan@uitm.edu.my (C.S.Y. Tan).

https://doi.org/10.1016/j.jece.2026.122337
Received 22 November 2025; Received in revised form 19 March 2026; Accepted 20 March 2026
Available online 21 March 2026

environmental degradation [1]. Moreover, urbanization and climate change are exacerbating global water scarcity and soil degradation [2,3]. As agricultural output is intrinsically linked to water availability, accounting for 70% of global freshwater withdrawal, water use optimization across farming systems is one of the central objectives in addressing global food security and climate resilience [4,5].

Water-retention agents (WRAs) are a type of soil additive applied directly to the soil to promote water storage and moisture retention for a longer duration, reduce water runoff and evaporation, and improve the soil structure, particularly in water-stressed regions [6]. The WRAs, such as superabsorbent hydrogels or polymers (SAHs or SAPs), generally can quickly imbibe and retain large quantities of water during rain or irrigation [7,8], and slowly release water for crop utilization when the soil is dry and short of water. This functionality improves drought resistance among crops, improve water use efficiency and reduce irrigation frequency. The SAHs can be derived from natural or synthetic resources and typically contain chemical groups, such as -NH_2, –OH, and –COOH [9]. Polysaccharide-based SAHs have emerged as biodegradable and sustainable materials for agricultural water management [10,11] and are commonly formulated as single network or semi-IPN systems. Nonetheless, their practical application may be constrained by insufficient mechanical durability and environmental adaptability, particularly under saline conditions, leading to rapid biodegradation in soil, which may necessitate frequent reapplication and increase costs [12]. Recent studies have demonstrated the effectiveness of hydrophilic polymer networks and hydrogel–biochar composites based on poly (acrylate-*co*-acrylamide) and poly(vinyl alcohol) in enhancing soil moisture retention and controlled-release applications [13–15].

In recent years, biochar is gaining popularity as a soil conditioner in sustainable agriculture and within the broader framework of a zero-carbon circular economy, owing to its intrinsic properties such as high surface area, favourable C/N ratio, abundant functional groups and capacity to enhance soil health and water holding capacity [16–19]. Biochar is a carbon-rich and highly porous material produced from biomass via pyrolysis. Despite these beneficial attributes, direct application of biochar in soils can involve practical considerations related to handling and performance consistency. Depending on feedstock and pyrolysis conditions, biochar may exhibit variable wettability and moisture/nutrient retention performance. Fine biochar particles may be susceptible to wind dispersion during field deployment [18,20,21]. These considerations motivate the integration of biochar into polymeric matrices, where immobilization within a hydrogel network reduces particle dispersion while promoting more consistent functional performance.

In addition, integrating biochar particles as fillers in hydrogels produces hydrogel composites with improved mechanical integrity and durability, water permeability, enhanced water retention, and cation exchange capacity under variable environmental conditions [5,22–24]. Beyond physico-chemical benefits, the porous biochar in the hydrogels can support microbial colonization and activities in the composites, which can further promote soil health and degradability of synthetic polymer matrices such as poly(acrylic acid) and poly(acrylamide) [25], offering synergistic benefits of SAHs and biochar. Palm kernel shell (PKS) biochar was selected in this study due to its structural and sustainability advantages. PKS is a locally abundant by-product of the oil palm industry in Malaysia, and their conversion into biochar supports agricultural waste valorisation. Compared with low-density wood-derived biochars and silica-rich rice husk biochar that primarily enhance porosity, PKS biochar possesses higher carbon density and intrinsic rigidity, allowing it to act as an effective reinforcing filler within polymer networks [26,27], thus improving network resilience during repeated swelling–deswelling cycles.

Most studies relied on experimental characterization and kinetic modelling, such as the Korsmeyer–Peppas model, to evaluate water absorption-retention and swelling characteristics of different hydrogel–biochar composites [5,28–30]. Few optimization techniques studies used the traditional one-factor-at-a-time (OFAT) approach to optimize water absorption of hydrogels and hydrogel composites [31,32], which often requires more experimental runs and is limited in accuracy [33,34]. Response Surface Methodology integrated with Central Composite Design (RSM-CCD) is a statistical tool that enables simultaneous evaluation of multiple process variables, development of predictive models, and identification of synergistic effects, thereby overcoming the limitations of OFAT optimization [33]. Although RSM has been widely applied to optimize the water retention performance of hydrogels [35–37], its application in the optimization of biochar-based systems remains comparatively limited [38].

To address these limitations while improving sustainability, this study develops double network hydrogel-biochar composites (DNHBCs) based on potassium poly(acrylate-*co*-acrylamide) (P(AA-*co*-AM)), poly (vinyl alcohol) (PVA) and PKS biochar (BC). By integrating a brittle first network with a flexible second network, double network hydrogels exhibit exceptional toughness and multifunctionality, making them unique among engineered hydrogel systems [39,40]. The integrated design of the DNHBC was guided by complementary functional performance with reduced synthetic polymer content and environmental compatibility for repeated irrigation cycles. The AM units, PKS BC and PVA secondary network can help the hydrogel composite maintain water uptake, structural resilience, porosity as well as soil compatibility, while reducing excessive ionic crosslinking of acrylate groups. This work focuses on optimizing structural formulation variables (methylene bisacrylamide (MBA) crosslinker, PVA, and BC loadings) using the RSM-CCD. This approach enables control of first-network crosslink density, secondary-network reinforcement and composite porosity, respectively, while maintaining constant monomer composition and neutralization degree to isolate structural effects. To the best of our knowledge, this work represents one of the first systematic attempts to employ the RSM-CCD approach for optimizing hydrogel–biochar composites. Effects of pH and multivalent cation solutions on equilibrium water absorption (EW) of the DNHBCs were also assessed to simulate varying soil conditions. The alkaline-treated BC and synthesized DNHBCs were characterized by using Fourier-Transform Infrared Spectroscopy (FTIR), Thermogravimetric Analysis (TGA), Scanning Electron Microscopy (SEM), and contact angle goniometer. The DNHBCs were designed to exhibit high EW in aqueous media under varying pH and cations while maintaining their structural robustness and reswelling capability, making them competitive WRAs. This work is deliberately positioned as a materials development and optimization investigation, focusing on the DNHBC composite's structure, intrinsic swelling behaviour, repeated and salinity tolerance as essential prerequisites for subsequent soil-based applications.

2. Methodology

2.1. Materials

Poly(vinyl alcohol) (PVA, molecular weight of 130,000 g/mol, analytical reagent (AR) grade), acrylic acid (AA, AR grade, 99%), acrylamide (AM, GC grade, $\geq$ 98%) and *N,N*-methylene bisacrylamide (MBA, AR grade, 99%) were purchased from Sigma Aldrich. Potassium hydroxide (KOH, AR grade, 85%), sodium hydroxide (NaOH, AR grade), hydrochloric acid (HCl, 37%, AR grade) and ammonium persulphate (APS, 98%, AR grade) were purchased from HmbG Chemicals and Acros Organics, respectively. Solvents, such as acetone (99.5%) and ethanol (99.7%) were of AR grade and were purchased from R&M Chemicals. NaCl (99%, J.T. Baker, USA), KCl (99%, J.T. Baker, USA), $CaCl_2$ (95%, HmbG Chemicals, China) and $FeCl_3$ were of AR grade, and their solutions were prepared using DI water.

2.2. Preparation of PKS biochar (p-BC)

The pristine PKS-derived biochar (denoted as p-BC) was produced

using a continuous microwave pyrolysis system. The PKS was directly fed into a quartz reactor positioned within a microwave cavity, which was operated at 2.4 GHz and 1 kW, through a screw conveyor system. Direct microwave heating whilst maintaining a stable pyrolysis temperature between 500 – 600 ºC ensures efficient thermal decomposition, which is critical to produce desirable biochar. The self-purging mechanism of microwave pyrolysis eliminates the requirement for external nitrogen or other carrier gases. Volatile compounds released from PKS interacted within the confined microwave cavity, while the limited-oxygen environment ensured proper pyrolysis conditions. The resulting solid p-BC was then discharged using a screw auger for subsequent collection and cooling.

2.3. Alkaline treatment of p-BC

Biochar tends to exhibit water-repellent properties owing to the presence of organic materials on its surface, which may cause poor interfacial adhesion within hydrophilic polymer matrices, such as potassium polyacrylate and polyacrylamide. Herein, p-BC was grounded and sieved by using a 425-micron sieve. The p-BC was treated with KOH solution (3 M) in a round-bottom flask at 1:10 (w/v) ratio according to the method by Li and coworkers [41]. The biochar suspension was stirred for 3 h at 60 °C and was washed with copious amount of DI water and ethanol until pH 7 and oven dried. Residual KOH was removed via neutralization of treated BC because neutral BC is preferred for soil application. The post KOH-treated BC is denoted as BC.

2.4. Syntheses of DNHBC and DNH

Synthesis of DNHBC consisting of P(AA-*co*-AM), PVA and BC was carried out via a one-pot free radical polymerization in DI water as illustrated in Fig. 1, in which APS and MBA were used as thermal initiator and crosslinking agent, respectively. PVA (1 – 3% w/v) was dissolved in DI water (20 mL) at 90 – 100 °C overnight in a 50-mL round bottom flask to completely dissolve PVA. The dissolved PVA was left to cool down before adding the monomers. AA (4.00 g, 55.52 mmol) was neutralized with KOH (8 M, 4.20 mL) in a 50-mL round bottom flask in an ice water bath to obtain 60% neutralized AA. At the end of reaction, DI water (2.80 mL) was added to the solution (pH 5 – 6) under continuous stirring in the ice bath until pH 7 was achieved.

The 60% neutralized AA and AM mixture was then added with MBA (0.3 – 0.7 wt% relative to total monomer content) and APS (0.08 g, 0.35 mmol) and stirred to dissolution. Subsequently, the PVA solution was added to the monomeric mixture, followed by BC (1 – 3% w/v), DI water (8 mL) and purged with N_2 for 30 min under continuous stirring at room temperature. The mixture was heated to 70 °C in the N_2 atmosphere for 7 h to complete the polymerization. After that, the semi-interpenetrating polymer network (semi-IPN) was cooled down and subsequently subjected to cyclic freeze-thaw treatment to form DNHBC. The prepared semi-IPN hydrogels were frozen at −24 °C for 16 h, followed by thawing at ambient laboratory temperature (25 ± 2 °C) for 8 h to ensure complete melting and structural relaxation [42]. This freeze–thaw cycle was repeated three times to promote physical crosslinking and formation of the secondary network. The resulting DNHBC was washed with some DI water and acetone to remove unreacted reactants and then dried at 70 – 80 °C until constant weight.

For comparison purposes, a double network hydrogel without BC (denoted as DNH) was synthesized under similar polymerization conditions as the DNHBC. The DNH was synthesized by using 60% neutralized AA, 0.5 wt% of MBA crosslinker and 2% w/v of PVA, while maintaining the other synthetic compositions.

2.5. Characterization

Chemical functionalities of BC, DNH and DNHBCS*x* composites were analyzed using an Attenuated Total Reflectance-Fourier Transform Infrared (ATR-FTIR) (Perkin Elmer, Frontier) between 4000 cm^{-1} and 600 cm^{-1}. The dried polymers were fully dissolved in D_2O and analyzed using a NMR Spectrometer (Bruker 400 MHz). Thermogravimetric analysis was carried out using a Perkin Elmer Pyris 1 TGA system with a nitrogen flow rate of 20 mL/min between 50 °C and 700 °C to analyze the thermal properties of DNHBCs according to the ASTM E1131–20 method (ASTM, 2020). The surface hydrophilicity of BC was evaluated by static sessile-drop contact angle measurements using a contact angle goniometer (HuiNuo, JINHE JY-PHb). BET surface area and pore structure were determined using a Micromeritics 3Flex surface area and porosity analyzer (Micromeritics Instrument Corp., USA). Prior to analysis, samples were degassed under vacuum at 200 °C for 8 h to remove moisture and volatile impurities. Nitrogen adsorption–desorption isotherms were measured at 77 K. The specific surface

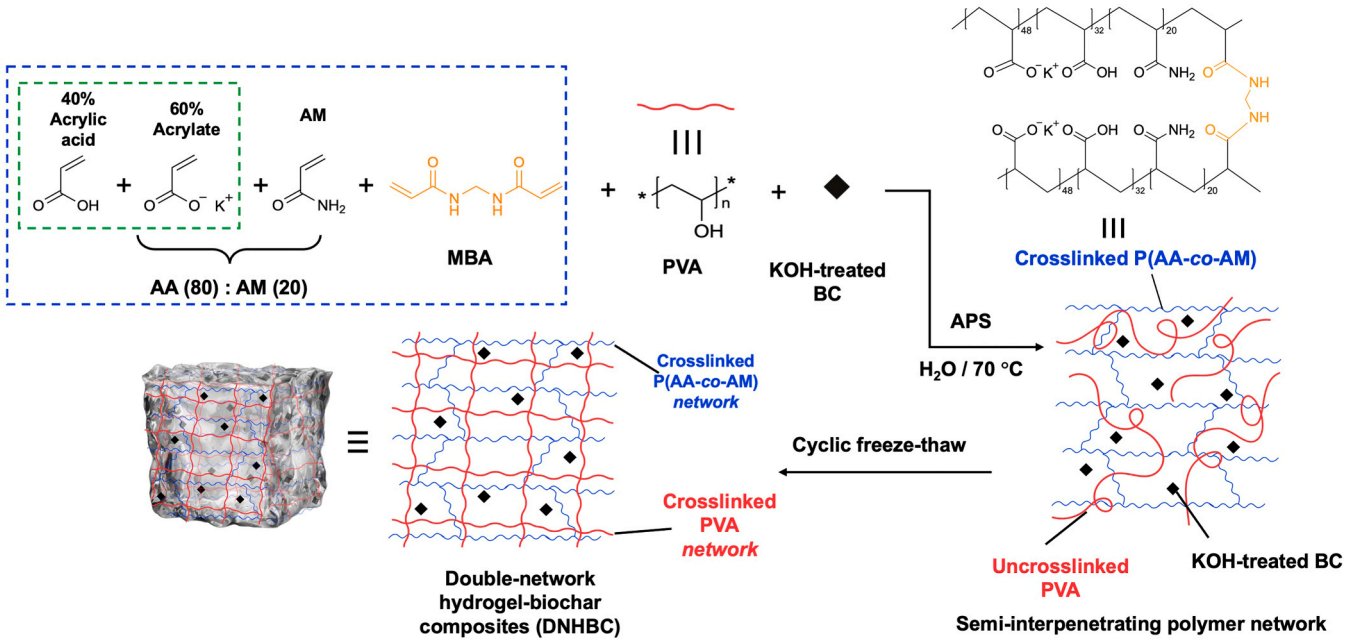

Fig. 1. Schematic synthesis of double network hydrogel-biochar composites (DNHBC).

area was calculated using the Brunauer–Emmett–Teller (BET) method within the relative pressure range of 0.05–0.30. Total pore volume was obtained at $P/P_o \approx 0.99$. Micropore characteristics were evaluated using the t-plot method. A droplet of DI water was carefully placed on the sample surface and the contact angle (°) was recorded. The surface morphologies of BC, DNH and DNHBC were observed under a Field Emission Scanning Electron Microscope (FESEM, JEOL JSM-7600F) after being sputtered with gold.

2.6. Water absorption optimization of DNHBCSx by RSM-CCD

Equilibrium water absorption (EW) of DNHBCs was optimized via the RSM-CCD using the Design Expert 13 Software. RSM-CCD is recommended for optimization since it incorporates full/fractional factorial design, centre points and axial points, allowing the experimentation of extremely high (+α) and low (-α) factor values that exceed the normal experimental range which can detect the curvature or quadratic effects and accuracy of the mathematical model [43]. Three independent experimental variables used in the structural optimization were the MBA crosslinker (X_1, wt%), PVA (X_2, % w/v), and BC (X_3, % w/v) and EW was the experimental response. The EW as well as swelling property of hydrogel-based materials are influenced by synthetic compositions, including concentrations of monomer, polymer and crosslinking density [44,45]. The experiments were designed through twenty DNHBC compositions (represented as DNHBCS*x* from this section onwards, where S*x* ($x = 1, 2\ldots. n$) indicates the experimental number generated by the software) considering different values for the independent parameters. These variables ranged from lower (-1) to upper limits (+1) as shown in Table 1. The EW of DNHBCS*x* was determined in two aqueous media, namely DI water and 0.9% w/v NaCl solution and suitable mathematical models were proposed [46–48].

The EW of DNHBCS*x* was analyzed by gravimetric method. First, dried DNHBCS*x* (0.10 g) was sealed in a nylon bag and soaked in DI water (100 mL) for 24 h at 25 °C until swelling equilibrium was reached. After that, the DNHBCS*x* was removed and surface water on the DHNBC was wiped dry before weighing. The EW of the hydrogels was calculated by using Eq. 1. The EW determination for DNHBCS*x* was repeated in 0.9% w/v NaCl solution.

$$\text{Equlibrium water absorption, } EW(g/g) = \frac{W_s - W_d}{W_d} \quad (1)$$

where W_s is the weight of swollen DNHBCS*x* and W_d is the weight of dried DNHBCS*x*.

2.7. Swelling kinetics

To investigate the swelling kinetics of DNHBCS*x*, time-dependent water absorption was evaluated by immersing the dried DNHBCS*x* (0.10 g) in DI water (100 mL) at 25 °C for 24 h. At predetermined time intervals, the DNHBCS*x* was removed and gently blotted to remove surface water and then weighed. The EW of DNHBCS*x* at each time interval was calculated by using Eq. 1. All measurements were performed in triplicate.

Table 1
Experimental factors and level used in RSM-CCD.

Independent variables	Symbol	Range and levels				
		-α = -1.68	-1	0	+ 1	+ α = +1.68
X_1: MBA (wt%)	A	0.1636	0.3	0.5	0.7	0.8364
X_2: PVA (% w/v)	B	0.3182	1	2	3	3.6818
X_3: BC (% w/v)	C	0.3182	1	2	3	3.6818

2.8. Water absorption performance in different pH and salt solutions

Based on the RSM-CCD analysis, two DNHBCS*x* with desirable EW and structural integrity in their swollen state were selected to further investigate their EW properties in Phosphate Buffer Solution (PBS) of different pH values (Table 2), tap water and salt solutions to simulate soil environment. Soil pH can influence EW of hydrogel composites, thereby influencing their swelling behaviour and ultimately regulating the release rate of water and encapsulated nutrients. The pH of PBS was adjusted with 0.1 M HCl and 0.1 M KOH to obtain the desired pHs. The dried DNHBCS*x* (0.10 g) was sealed in a nylon bag and soaked in the PBS solution (100 mL) separately for 24 h at 25 °C to reach swelling equilibrium. After that, the DNHBCS*x* was removed from the aqueous solution, surface water of hydrogel was wiped dry and weighed.

The EW of DNHBCS*x* was further evaluated separately in tap water and 0.9% w/v salt solutions (NaCl, KCl, $CaCl_2$ and $FeCl_3$). The EW of the hydrogels was determined in triplicate according to Eq. 1. Structural stability of DNHBCS6 was evaluated and compared with DNH (control) through dimensional change and cyclic reswelling tests, where cylindrical samples maintained their shape after repeated wetting–drying cycles, implying sufficient integrity for soil water-retention applications. Briefly, as-prepared DNHBCSx and DNH cylinders were first immersed in DI water and 0.9% w/v salt solutions (NaCl, KCl, $CaCl_2$ and $FeCl_3$ for 24 h at ambient conditions in Step 1, followed by re-immersion of the saline-treated cylinders in fresh batch of DI water in Steps 2 and 3 to observe EW, EW recovery and volume changes. The volume of the cylindrical hydrogels was calculated based on their diameters and height measured using a vernier caliper.

2.9. Reswellability and structural durability experiments

Reswellability experiments were carried out in triplicate up to three consecutive swelling–drying cycles to evaluate the water uptake capacity and assess the structure and weight loss of the spent DNHBCS*x*. The dried DNHBCS*x* (0.10 g) was soaked in DI water (100 mL) at 25 °C until swelling equilibrium. The swollen DNHBCS*x* was removed and gently blotted to remove surface water prior to weighing. In the water desorption process, the swollen DNHBCS*x* was oven dried between 45 and 70 °C until constant weight to complete the first wetting-drying cycle (denoted as Cycle 1). The EW for each cycle was calculated using Eq. 2. The structural durability of the DNHBCS*x* was evaluated based on the material weight loss (%) during the swelling-drying cycles using Eq. 3. This experiment was also conducted for DNH for comparison. In addition, the cyclic reswellability test was repeated using as-prepared cylindrical DNHBCS*x* and DNH samples to compare dimensional stability and structural evolution alongside EW performance.

$$\text{Equlibirum water absorption, } EW(g/g) = \frac{W_s - W_t}{W_t} \quad (2)$$

$$\text{Weight loss}(\%) = \frac{W_o - W_t}{W_o} \times 100\% \quad (3)$$

where W_s is the weight of swollen DNHBCS*x* at respective cycles, W_t is the weight of oven-dried DNHBCS*x* and W_o is the initial dry weight of DNHBCS*x*.

2.10. Water holding capacity measurement

The water holding capacity (WHC) of DNHBCSx refers to the volume

Table 2
Solution pH used in the EW of DNHBCS*x*.

Aqueous Media	Acidic PBS	Neutral PBS	Basic PBS
pH value	3 – 4	7	8 – 9

of water retained in the soil after drainage. This experiment evaluated the potential application of DNHBCS*x* composites as WRAs. The WHC was investigated in two types of soils (sandy loam and clay loam), which were sieved and oven dried. Preparation of the soil is described in Supplementary Information S1 (Table S1). The dried soil from each type (40.00 g) was mixed thoroughly with DNHBCS*x* (0.80 g, 2% w/w) in plastic containers (Φ 5.5 cm × H 7.5 cm) with perforated bottoms lined with filter paper. Additionally, control containing each type of soil only, without the addition of DNHBCS*x* was included for comparison. Each sample was supplemented with DI water (200 mL) until the soil was fully saturated, with no visible surface ponding observed. The plastic containers containing the hydrogel composite and soil were then covered to prevent water loss from evaporation, while allowing drainage for 24 h. After drainage, the mass of each sample was measured and WHC was calculated according to Eq. 4 [23]:

$$\text{Water holding capacity, WHC}(\text{g}/\text{g}) = \frac{m_t - m_s - m_{WRA}}{m_s + m_{WRA}} \quad (4)$$

where m_t is the total wet mass of the sample after being left to drain for 24 h, m_s is the dry mass of the soil, and m_{WRA} is the dry mass of the hydrogel composite.

2.11. Water retention capacity measurement

In the subsequent water retention capacity (WRC) measurement, DNHBCS*x* (2% w/w, 0.80 g) was mixed with each soil type (40.00 g) at a hydrogel composite-to-soil ratio of 1:50 in the plastic containers (Φ 5.5 cm × H 7.5 cm). The control experiment was carried out without the addition of DNHBCS*x*. DI water was added to each container, consisting of the DNHBCS*x*-soil mixture, with the total volume of DI water equating to 100% WHC of each soil. For clay loam, excess water was removed using a blotting technique until the target moisture level was reached. The perforated containers were then covered with clingfilm to prevent any drainage, ensuring that water loss occurred only through evaporation. The samples were kept at room temperature (24.7 – 31.7°C) with relative humidity (RH) of 63–94%. The mass of the samples was recorded at specified time intervals using the gravimetric method. The experiment was conducted in triplicate and WRC was calculated using Eq. 5 [23]:

$$\text{Water retention capacity, WRC (\%)} = \frac{m_t - m_d}{m_o - m_d} \times 100 \quad (5)$$

where m_t is the total mass of the wet sample at day t, m_d is the dry mass of the sample prior to water addition, and m_o is the initial mass of the wet sample.

3. Results and discussion

3.1. Fourier transform infrared (FTIR) and NMR analyses

Double network hydrogel-biochar composites (DNHBCs) and double network hydrogel (DNH) in the absence of biochar were prepared via

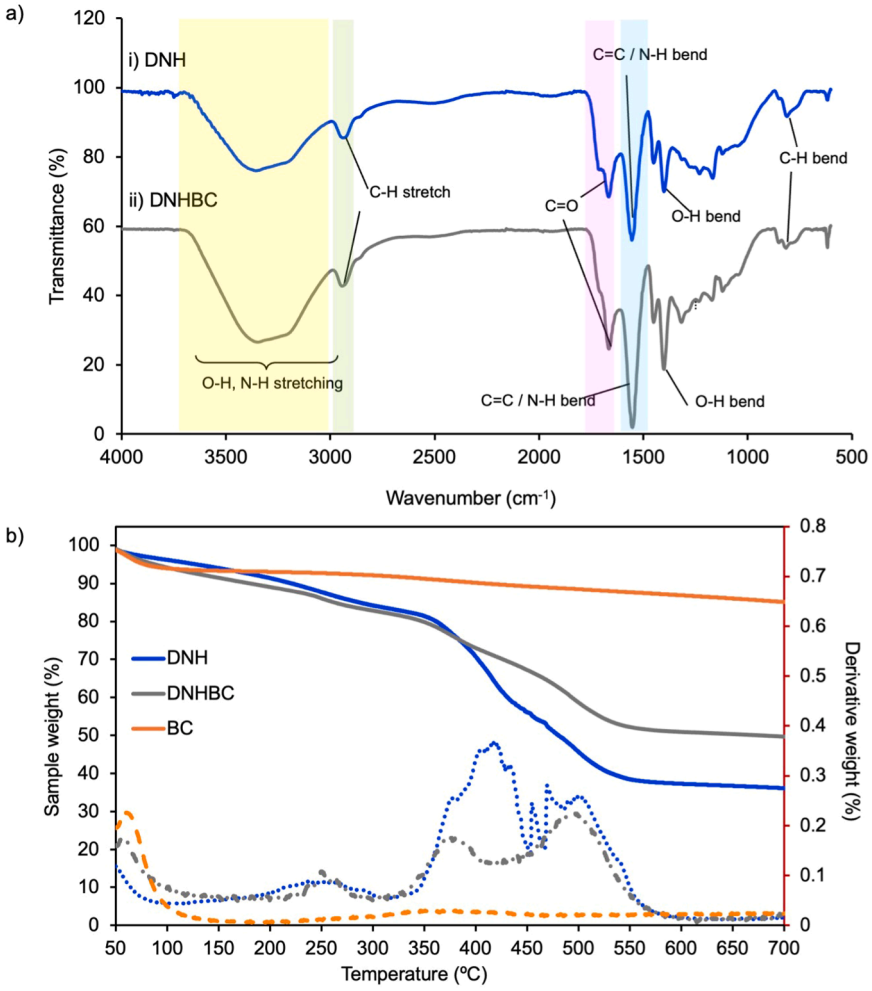

Fig. 2. (a) FTIR spectra of (i) DNH and (ii) DNHBC. (b) Comparison of TG (primary y-axis, solid lines) and DTG curves (secondary y-axis dotted lines) for DNHBC, DNH and BC.

solution polymerization and cyclic freeze-thaw. The crosslinked double network structures of DNHBC and DNH were obtained after the cyclic freeze-thaw. Fig. 2a illustrates FTIR spectra of DNHBC and DNH, while the FTIR spectra of the untreated (p-BC) and treated biochar (BC) are depicted in Figure S1. Table S2 summarizes the chemical functional groups and their peak wavenumbers for p-BC, BC, DNH and DNHBC. In Figure S1b, a broad and intense OH band at 3000 – 3700 cm^{-1} was observed in BC after the KOH treatment, which was absent in the FTIR spectrum of more hydrophobic p-BC (Figure S1a). This suggests the conversion of hydroxyl and carboxyl groups in p-BC to more polar and hydrophilic acrylate (–COO–K^+) and alkoxide (–O–K^+) in the KOH-treated BC, enhancing the BC's affinity for water and hydrogen bonding formation [49]. The intense peaks in the region of 900 – 1300 cm^{-1} are mostly likely attributed to oxygen functional groups in biochar, such as –C–O–C and –Si–O bands [50], while the peaks between 1500 – 1600 cm^{-1} represent the aromatic C═C and C═O [51,52]. Alkaline treatment can modify the surface properties of any biochar, making it more hydrophilic via increased number of oxygen-containing functional groups, which is necessary for enhancing the interactions between BC and superabsorbent hydrogels [41,50].

Fig. 2a shows the FTIR spectra of DNHBC and DNH. The C═O stretch and N–H bending vibration showed characteristic absorption between 1450 – 1700 cm^{-1} in both DNHBC and DNH, which confirms the successful copolymerization of potassium acrylate, acrylic acid, acrylamide and methylene bisacrylamide to form the crosslinked P(AA-*co*-AM) network [53], which is supported by the NMR spectra of crosslinked P(AA-*co*-AM) in Supplementary Information S3 (Figure S2). Superposition of amide group (1552 – 1555 cm^{-1}) and C═O in carboxyl group resulted in the band shift of C═O stretching vibration (1663 cm^{-1}) in DNH and DNHBC, suggesting the formation of strong hydrogen bonds between –COOH and –$CONH_2$ [54]. The peak at 1401 cm^{-1} is attributed to the -COO^- and C-O stretchings as well as O-H bending within the DNHBC and DNH. [55]. All characteristic peaks of BC were observed in the IR spectrum of DNHBC. Due to the presence of BC in the DNHBC, the C–H intensity in DNHBC decreased, which agrees with Wu et al. [52] who reported lower transmission in the IR spectra for composites containing higher BC dosage. This observation suggests enhanced molecular vibrations and/or complexity of DNHBC structure, following the successful inclusion of KOH-treated BC within the DNHBC composite. Both DNHBC and DNH showed broad O–H stretching overlapped with –NH peak of amide at 3200–3300 cm^{-1}, with DNHBC exhibiting a more intense broad peak than that of DNH, most likely attributed to BC. The peaks between 2900 cm^{-1} and 2960 cm^{-1} are attributed to the symmetric and asymmetric stretching vibrations of CH_2 groups in the polymeric backbone of DNH. The FTIR results confirm the successful incorporation of KOH-treated BC into the DNH matrix owing to enhanced hydrogen bonding and interfacial compatibility contributing to improved hydrophilicity and structural integrity of the resultant hydrogel composite.

3.2. Thermogravimetric analysis (TGA)

The TG-DTG results for DNHBC, DNH, BC and p-BC are presented in Fig. 2b, Figure S3 and summarized in Table S3 (Supporting Information S4), showing the weight losses of each material as a function of temperature. Initial weight losses between 50 °C and 100 °C for p-BC, BC, DNH and DNHBC correspond to the moisture evaporation, solvent loss and other volatile components. Figure S3 shows slight variations in thermal stability and weight loss of BC and p-BC. The small decomposition peak at 370 °C in BC was probably due to residual KOH in the BC. The minimal weight loss in the p-BC and treated BC within the similar temperature window possibly indicates their stable carbon structure.

Distinct thermal degradation stages in the TG-DTG curves for DNHBC and DNH (Fig. 2b) suggest modification of thermal degradation profile of DNHBC owing to the BC inclusion in the DNH's matrix. The shift and reduced intensity of the decomposition peaks were accompanied by a lower decomposition rate in DNHBC between 200 °C and 600 °C, arising from loss of functional groups and decomposition of the hydrogel composite. The slower decomposition rate indicates that strong intermolecular interactions (e.g., hydrogen bonding and electrostatic interactions) between BC particles and DNH have substantially reinforced the bulk structure and thermal stability of DNHBC compared to its pristine DNH [53,56], corroborating the findings of Petousis and coworkers involving olive tree biochar-polypropylene composites [57]. A higher final weight (%) in DNHBC was expected owing to the addition of BC in the hydrogel composite. TGA results suggest that enhanced thermal stability arises from strong intermolecular interactions within the DNHBC composite and the pore-filling reinforcement effect of BC particles embedded in the DNH matrix.

3.3. Contact angle and BET characterizations

The wettability of a material can be evaluated via contact angle analysis, which provides direct insight into its surface hydrophilicity. Fig. 3a-b depict the contact angles of BC and p-BC. The contact angles of the KOH-treated biochar (BC) and pristine biochar (p-BC) were 82.03° and 101.40°, respectively. Low-temperature KOH washing at 60 °C enhances the surface negative charge and polarity by deprotonating oxygenated groups through removal of surface impurities and pore cleaning. The enhanced surface wettability of BC not only promotes better compatibility and dispersion of BC within DNHBC matrix but favours water immobilization within the polymer–biochar interface. This result is consistent with the increased hydrophilicity reported for the KOH-treated rice husk biochar by Li et al. [41].

The nitrogen adsorption–desorption analysis (Table S4) showed highly microporous p-BC and BC with micropores contributing 95% of the total BET surface area and ~93% of the total pore volume. Notably, the average pore diameter remained constant at ~2.0 nm, indicating that the treatment did not induce pore generation or pore destruction. The slight reductions in the S_{BET} and V_{tot} observed for BC could be attributed to reduced nitrogen accessibility, arising from pore-mouth narrowing or partial blockage of micropores following KOH washing.

BC acts as a dispersed filler within a continuous hydrophilic hydrogel matrix of DNHBC composites. Although BC particles may retain partially hydrophobic domains, the hydrogel-rich DNHBC surface dominates overall wetting property, leading to observed low contact angles (Fig. 3c-d). Moreover, the double network hydrogel architecture helps prevent polymer network collapse under hydrated conditions. The slightly higher contact angle observed for DNHBCS18 (46°) is consistent with its twofold higher PVA content (2% w/v), which likely reduces its

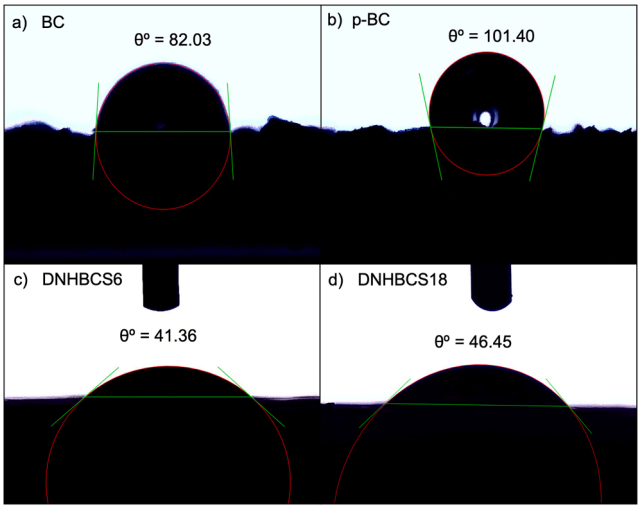

Fig. 3. Contact angle analyses of (a) BC; (b) p-BC; (c) DNHBCS6 and (d) DNHBCS18.

surface water uptake at the outermost surface.

3.4. RSM-CCD optimization for equilibrium water absorption

Table 3 presents twenty experimental conditions generated by the Design Expert 13 software. Each experiment corresponds to a row in the matrix with its specific process conditions (denoted as DNHBCS*x*) and was conducted in duplicate in two aqueous media. From the 20 experimental runs, only 17 experiments were selected in our study, while 3 experimental samples were excluded from data analysis owing to statistical outlier(s) in the dataset as detailed in Supporting Information S5. Inclusion of these data points significantly distorted the model fit and compromised the accurate determination of optimal conditions [58]. The EW responses of DNHBCS*x* in DI water and 0.9% w/v NaCl were fitted to an empirical second-order quadratic polynomial model equation (Eq. 6):

$$Y = \alpha_0 + \sum_{i=1}^{3} \alpha_i X_i + \sum_{i=1}^{3} \alpha_{ii} X_i^2 + \sum_{i=1}^{3} \sum_{j=1}^{2} \alpha_{ij} X_i X_j \quad (6)$$

where, Y, α_0, α_i, α_{ii}, and α_{ij} are the predicted response, constant, linear, quadratic, and interaction coefficients, respectively. The input variables, experimental, and software generated responses are shown in Table 3.

The relevance and acceptability of the empirical second-order quadratic polynomial model (Eq. 6) for the EW responses of DNHBCS*x* was confirmed by ANOVA, sequential model sum of squares, model summary statistics tests (*p*-value and *F*-value) and lack of fit tests (Table 4, Tables S5 – S7). The quadratic model fitted well with the EW data in both aqueous environments. The p-values for the EW of DNHBCS*x* in both aqueous media were less than 0.05 with high F-values. The F-values observed were 33.18 ($p < 0.0001$) and 15.48 ($p = 0.0008$) in DI water and 0.9% w/v NaCl, respectively (Table 4), showing the significance of the model and high confidence level of more than 95%. Moreover, the Lack of Fit (LOF) analysis (Table S7) was higher than 0.05 and insignificant relative to pure error (Table S6), which indicates the good predictability of the model used.

The coded equations for the polynomial model showing the relationship between the independent variables and EW response are expressed in Eqs. 7 and 8 using the empirical second-order polynomial Eq. 8. As shown in Table S7, the correlation coefficients (R^2) in both DI water and 0.9% w/v NaCl were 0.9771 and 0.9522, respectively, with both R^2 values in good agreement with their adjusted R^2 values of 0.9477 (DI water) and 0.8907 (0.9% w/v NaCl), corroborating strong correlations between the observed and projected values across both media. The observed R^2 must be greater than adjusted R^2 as a supporting evidence that the model is of high quality [59]. Moreover, the predicted R^2 values of 0.8164 (DI water) and 0.7066 (0.9% w/v NaCl) are in reasonable agreement with adjusted R^2 values with a difference of less than 0.2.

Table 3
Independent variables and EW of DNHBCS*x* in DI water and 0.9% w/v NaCl solution.

Experiment standard (S)	Run	X_1	X_2	X_3	EW Response	
		A: MBA dosage (wt%)	B: PVA dosage (% w/v)	C: Biochar dosage (% w/v)	DI water (g/g)	0.9% w/v NaCl (g/g)
6	**1**	**0.70**	**1.00**	**3.00**	**328.28**	**33.12**
7	2	0.30	3.00	3.00	75.96	16.93
19	3	0.50	2.00	2.00	252.51	30.38
10	4	0.84	2.00	2.00	84.06	21.20
14	5	0.50	2.00	3.68	295.70	30.98
5	6	0.30	1.00	3.00	419.74	41.10
18	**7**	**0.50**	**2.00**	**2.00**	**309.08**	**36.86**
15	8	0.50	2.00	2.00	277.68	38.54
8	9	0.70	3.00	3.00	202.58	25.64
13	10	0.50	2.00	0.32	53.22	17.98
12	12	0.50	3.68	2.00	190.65	24.35
9	13	0.16	2.00	2.00	69.49	16.42
20	15	0.50	2.00	2.00	303.12	35.05
4	16	0.70	3.00	1.00	179.53	24.23
11	18	0.50	0.32	2.00	477.89	52.39
2	19	0.70	1.00	1.00	105.32	21.59
1	20	0.30	1.00	1.00	291.61	37.08

EW in DI water (g/g)

$$= +284.94 - 84.00B + 61.15C + 70.14AB - 34.36BC - 70.9A^2 + 20.14B^2 - 36.36C^2 \quad (7)$$

EW in 0.9% w/v NaCl (g/g)

$$= +35.23 - 7.49B + 3.28C + 5.68AB - 5.98A^2 - 3.88C^2 \quad (8)$$

Referring to Table 4, the significant terms for the coded model in DI water are B, C, AB, BC, A^2, B^2 and C^2. In contrast, the significant model terms for the 0.9% w/v NaCl environment include B, C, AB, A^2 and C^2. To enhance the quality and simplify the mathematical models, the insignificant coefficients of both equations (A and AC for DI water, whereas A, AC, BC and B^2 for 0.9% w/v NaCl) are eliminated [46]. The regression coefficients with positive signs indicate a synergistic effect, whereas those with negative signs indicate antagonistic influences on the experimental response [59]. From Eqs. 7 and 8, the constants of 284.94 and 35.23 were not affected by any factors. The positive terms, such as C, AB and B^2 in Eq. 7, as well as C and AB in Eq. 8 denote variables that enhance the EW response. Conversely, the negative terms, such as B, BC, and C^2 (DI water), and B, A^2 and C^2 (0.9% w/v NaCl) suggest the increase in these factors reduces EW. Interestingly, the most influential parameter affecting EW in both media is PVA, with F-values of 95.66 (DI water) and 58.83 (0.9% w/v NaCl). This is followed by BC loading, with F-values of 50.69 (DI water) and 11.29 (0.9% w/v NaCl). As indicated in Eq. 7, EW is strongly governed by the negative effect of PVA (-84.00B) and positive effect of BC (+61.15 C). Comparable trends persist under saline conditions, although the EW values are approximately an order of magnitude lower owing to reduced electrostatic repulsion among ionized carboxylate groups and diminished osmotic swelling pressure (ionic shielding effects) (Eq. 8). The perturbation plots in Figures S4a and S5a both show similar trends, where parameter B (PVA, % w/v) has the highest deviation than A (MBA, wt%) and C (BC, % w/v) based on the reference point defined by the software.

The model validation was further assessed for these experimental results in Figures S4b and S5b. The normality plots of externally studentized residuals demonstrate maximum number of coloured points were clustered in a narrow range on the normal probability line, whilst the insignificant points were not positioned on the normal probability line. Additionally, every data point was within the residual limits (±4.81963) (Figures S4c and S5c), indicating the model's validity for EW in both aqueous media. Figures S4d and S5d further support the degree of conformity between the actual and predicted EW data, with all data points being scattered closely to the diagonal line, indicating a high degree of correlation between the actual and predicted values. These statistical analyses affirm that the quadratic models are well-suited for predicting the interactive influences of the independent factors on the EW responses of DNHBCS*x*.

The regression equations can be visualized using three-dimensional (3D) response surface plots to identify the optimal values of the variables and further elucidate the coupled interactions among the model parameters affecting EW or swelling behaviour of DNHBCS*x*. In these plots, two independent variables were varied, while the remaining variables were held constant [46,60,61]. As shown in Table 4, Eqs. 7 and 8, the A-B and B-C interactions were the only significant factors influencing EW in DI water, while the A-C interaction was deemed negligible due to its low F-value. In contrast, only A-B interaction demonstrated statistical significance for EW response in the saline environment. These two-factor interactions in response surface plots are depicted in Fig. 4.

Table 4
Analysis of Variance (ANOVA) of EW responses for DNHBCS*x* in (a) DI water and (b) 0.9% w/v NaCl solution.

a) DI water

Source	Sum of squares	df[a]	Mean square	F-value	p-value	Remarks
Model	**2.463E+ 05**	**9**	**27362.84**	**33.18**	**< 0.0001**[b]	**Significant**
A-MBA dosage	54.34	1	54.34	0.07	0.8048	Insignificant
B-PVA dosage	78876.46	1	78876.46	95.66	< 0.0001	Significant
C-Biochar dosage	41797.68	1	41797.68	50.69	0.0002	Significant
AB	28546.18	1	28546.18	34.62	0.0006	Significant
AC	379.12	1	379.12	0.46	0.5195	Insignificant
BC	6851.57	1	6851.57	8.31	0.0236	Significant
A^2	61849.73	1	61849.73	75.01	< 0.0001	Significant
B^2	4990.21	1	4990.21	6.05	0.0435	Significant
C^2	16268.17	1	16268.17	19.73	0.0030	Significant
Residual	5771.94	7	824.56			
Lack of Fit	3756.23	4	939.06	1.40	0.4078	Insignificant
Pure error	2015.71	3	671.90			
Cor Total	2.520E+ 05	16				

b) 0.9% w/v NaCl

Source	Sum of squares	df[a]	Mean square	F-value	p-value	Remarks
Model	**1486.17**	**9**	**165.13**	**15.48**	**0.0008**[b]	**Significant**
A-MBA dosage	2.59	1	2.59	0.2425	0.6375	Insignificant
B-PVA dosage	627.44	1	627.44	58.83	0.0001	Significant
C-Biochar dosage	120.41	1	120.41	11.29	0.0121	Significant
AB	187.46	1	187.46	17.58	0.0041	Significant
AC	0.7742	1	0.7742	0.0726	0.7954	Insignificant
BC	6.00	1	6.00	0.5626	0.4777	Insignificant
A^2	426.25	1	426.25	39.97	0.0004	Significant
B^2	13.05	1	13.05	1.22	0.3053	Insignificant
C^2	185.29	1	185.29	17.37	0.0042	Significant
Residual	74.65	7	10.66			
Lack of Fit	37.51	4	9.38	0.7573	0.6155	Insignificant
Pure error	37.15	3	12.38			
Cor Total	1560.82	16				

Note:
P-values less than 0.0500 indicate model terms are significant.
Values greater than 0.0500 indicate the model terms are not significant.
[a] Degree of freedom.
[b] Significance

In DI water, the positive MBA-PVA interaction (+70.14AB, Eq. 7) signifies that the influence of MBA crosslink density depends on the level of secondary network reinforcement. Increasing MBA promotes the formation of a denser primary polymer network with smaller pores, thereby limiting EW [62]. However, the extent of this restriction depends on the PVA content, as the secondary network further constrains chain mobility and pore accessibility. Together, MBA and PVA regulate the balance between osmotic swelling pressure and elastic restoring forces of DNHBCS*x*. Consequently, simultaneous variation of MBA and PVA produces non-additive effects on EW, as evidenced by the tilted curvature and non-parallel contour lines in the response surfaces (Fig. 4a). Meanwhile, the negative PVA-BC interaction (-34.36BC) suggests that although BC increases EW via its porous and hydrophilic nature [63], this benefit is diminished at higher PVA contents. Increased PVA promotes hydrogen bonding and crystalline domains, yielding a denser network that restricts water ingress and limits access to BC pores [64], as reflected in Fig. 4b. The regression model for 0.9% w/v NaCl (Eq. 8, Fig. 4c) retains a significant MBA-PVA interaction (+5.68AB). In contrast, the absence of a PVA-BC interaction term suggests the role of BC-related porosity and hydrophilicity when ionic screening dominates swelling behaviour. These interactions among formulation parameters reflect the combined influence of network elasticity, pore accessibility and ionization-driven swelling.

Post-swelling visual inspection was used as an application-relevant criterion to ensure the hydrogel composites retain cohesion and durability under soil loading and repeated hydration cycles. Despite possessing the highest EWs in DI water (> 400 g/g) and NaCl solution (40 – 53 g/g), the structural integrity of DNHBCS11 and DNHBCS5 appeared compromised, showing vulnerability to network rupture in swollen state owing to low degree of crosslinking (0.3 – 0.5 wt% MBA) and low PVA content (0.32 – 1% w/v) as the supporting matrix (refer to Table 2 for their compositions). Consequently, the third- and fourth-ranked DNHBCS6 and DNHBCS18 were selected, considering their high EW in DI water while retaining excellent structural integrity derived from the double network composite architecture [38,65–67]. Such structural robustness of double network systems is typically absent in SAHs consisting of single network hydrogels or semi-IPN [68]. The selection of these DNHBCS*x* composites was further justified by their EWs in both aqueous media, which consistently fall within or near the yellow-to-red response zone, associated with higher EW response (Fig. 4). Our selection strategy for the optimized experiments based on a practical standpoint coincides with the approach adopted by Iula and colleagues [69]. The optimal compositions consisting of 1 – 2% w/v PVA and 2 – 3% w/v BC as represented in DNHBCS6 and DNHBCS18 showed greater water absorbency and structural integrity, both of which are two integral attributes that underpin their potential as effective WRAs. Moreover, BC incorporation imparts supplementary soil conditioning effects.

3.5. Scanning electron microscopy (SEM)

Fig. 5 and S6 present the SEM micrographs of DNHBCS*x*, DNH and BC, respectively. BC is consisted of irregular carbonaceous particles with heterogenous surface texture and sharp edges (Figure S6a). Comparing the lyophilized as-prepared DNHBCS*x* composites (Fig. 5a-b) with the as-prepared DNH (Figure S6b), notable morphological improvements were observed with the BC inclusion. Unlike the shallow and sparse pores observed in the relatively smooth and dense DNH, which suggest lower porosity and restricted internal channels, the as-prepared

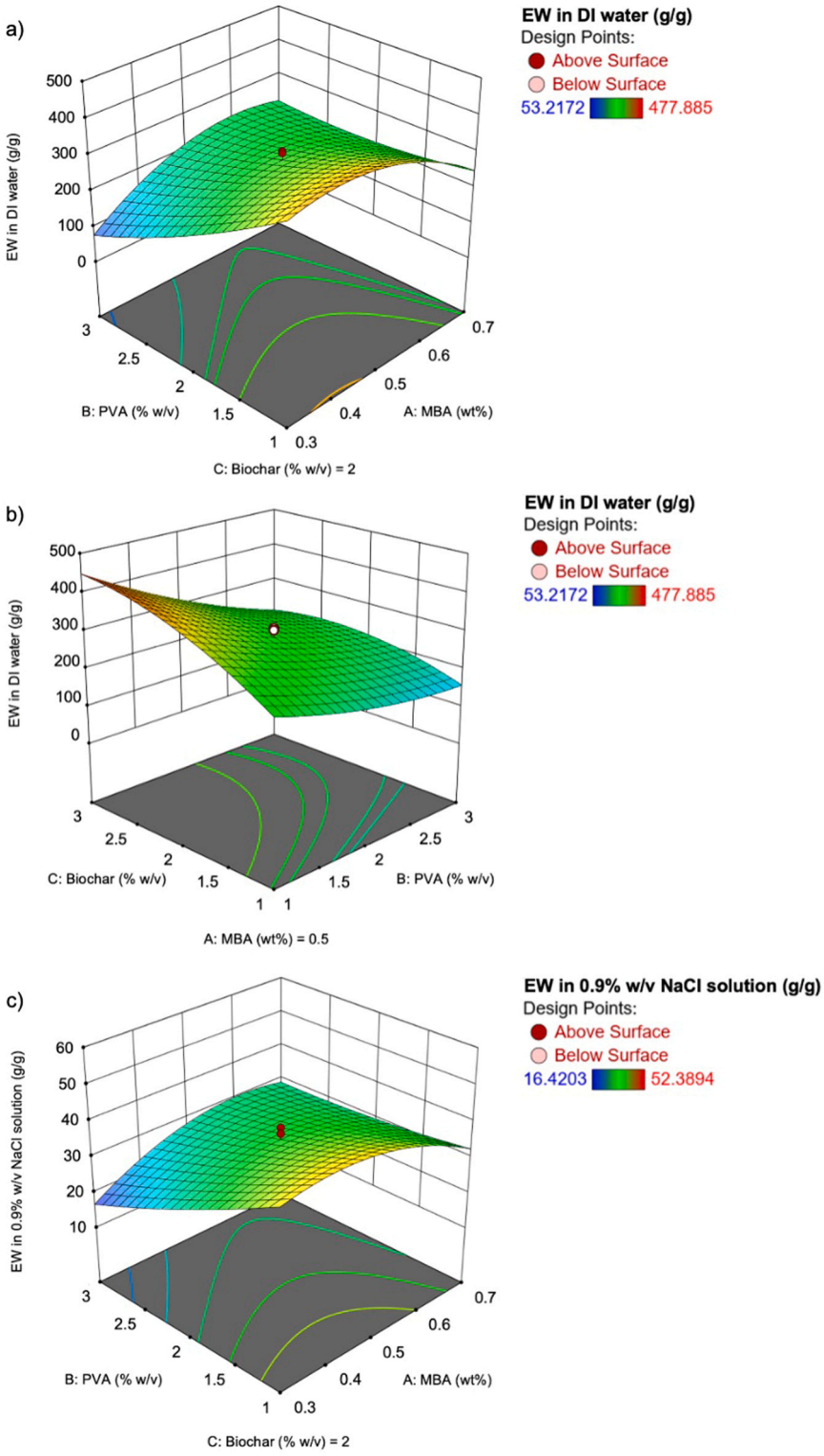

Fig. 4. Response surface plots of EW as a function of (a) MBA - PVA and (b) PVA - BC in DI water; and (c) MBA - PVA in 0.9% w/v NaCl.

DNHBCS*x* displayed more heterogenous and compact textures with enlarged, deeper and interconnected pores which are partially occupied by BC particles. The presence of BC not only enhances the porosity and surface roughness, but also contributes to improved structural stability by reinforcing the DNHBC matrix, which is not evident in the smoother pure DNH. The denser morphology observed in the as-prepared DNH and DNHBCSx samples is characteristic of freeze–thawed PVA networks, which are known to develop more consolidated and less porous structures after 2–4 freeze–thaw cycles [70]

A more porous morphology was observed in the swollen–then–freeze-dried DNHBCS*x* composites (Fig. 5c–d), reflecting their functional hydrated state. This approach captures network expansion, reopening of pore channels and preservation of structural integrity after water uptake, providing direct evidence of water transport pathways important for water retention. In the hydrated DNHBCS6, the combination of higher BC loading (3% w/v), higher covalent crosslinking

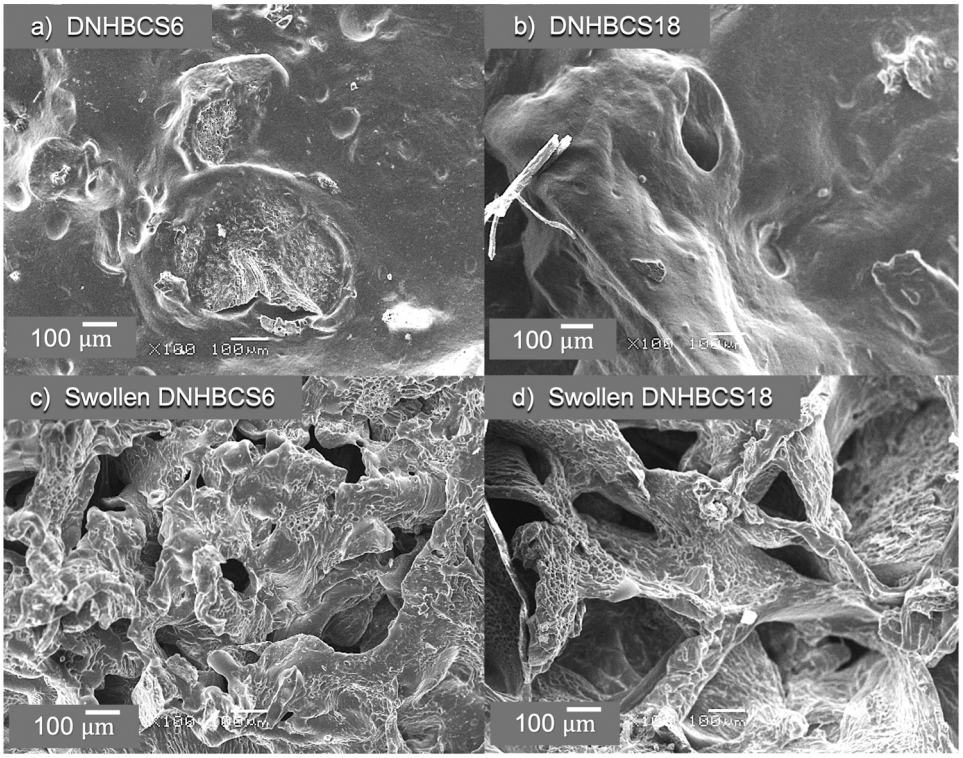

Fig. 5. SEM micrographs of freeze-dried as-prepared (a) DNHBCS6 and (b) DNHBCS18; and swollen-then-freeze-dried (c) DNHBCS6 and (d) DNHBCS18 at 100 × magnification.

density (0.7 wt% MBA) and lower PVA content (1% w/v) produced a more rigid and compact 3D network characterized by smaller pores and irregular internal channels, indicative of increased crosslink density. These confined channels may facilitate water retention in DNHBCS6 [71]. In contrast, the swollen-then-freeze-dried DNHBCS18 (2% w/v PVA, 2% w/v BC and 0.5 wt% MBA) exhibited a more open and interconnected network with larger pores, consistent with its lower crosslink density and reduced BC loading.

3.6. Swelling kinetics

Swelling rate is a critical determinant of hydrogel performance in soil retention and controlled-release applications, as it governs both the material's water uptake capacity and the diffusion-controlled release of water and encapsulated nutrients [5]. Fig. 6a-b illustrate the time-dependent swelling of DNHBCS*x* in DI water at ambient temperature for 24 h. Both DNHBCS6 and DNHBCS18 exhibited rapid water uptake within the first 6 h, achieving EW values of 271.24 g/g and 229.00 g/g, respectively, at 8 h. Notably, DNHBCS18 exhibited greater fragility in its fully swollen state, making it more prone to structural breakage, leading to lower EW compared to DNHBCS6.

The swelling kinetics of DNHBCS*x* composites were best described by the pseudo-second-order model with $R^2 \approx 0.99$ indicating relaxation-controlled swelling behaviour (Supporting Information S7, Figure S7, Table S8). This means that water uptake in DNHBCS*x* is governed by diffusion coupled with progressive polymer chain relaxation and network restructuring, a phenomenon typically reported in hydrogels and superabsorbent materials [13]. Diffusion exponents ($n = 0.79$–0.87) further reveal anomalous (non-Fickian) transport, where solvent diffusion and polymer relaxation occur concurrently. The slightly higher diffusion exponent for DNHBCS18 suggests enhanced polymer chain relaxation, potentially arising from increased PVA content and BC-induced structural reinforcement.

Overall, the swelling behaviour of DNHBCS*x* reveals a multi-phase water absorption mechanism, governed by the interplay between the hydrogel composites and its aqueous environment. Upon exposure to an aqueous environment, water molecules rapidly interact with the hydrophilic moieties, such as $–COO^-$, –COOH, –OH and $–CONH_2$ on the DNHBC's surface, facilitate swift surface hydration and initiate swelling as depicted by the time-dependent expansion of the hydrogel composites. Following surface hydration, the diffusion of water molecules into the internal polymer network is driven by osmotic gradients and capillary forces, resulting in the network expansion. Subsequent ionization of the carboxyl groups increases electrostatic repulsion and osmotic swelling pressure, while polymer chains gradually relax and undergo rearrangement, leading to progressive pore enlargement and water uptake until equilibrium is achieved within a day. Such diffusion–relaxation coupling pattern has been reported in P(AA-*co*-AM)/PVA hydrogel composites and related semi-IPN networks [13,72]. Nevertheless, the double network composite architecture stabilizes this expansion process. The PVA secondary network provides elasticity and structural integrity during swelling, while the porous BC introduces interconnected channels and internal pores that facilitate water transport and storage [22,73].

3.7. Effects of pH and salts on equilibrium water absorption capacities

Since the DNHBCS*x* incorporates both acrylic acid and acrylate groups with its polymeric structure, it exhibits pH-responsive behaviour that directly influences its EW capacity, as observed in other hydrogels containing acidic groups, such as –COOH [74]. Fig. 7a depicts the effects of pH on the EW performance of DNHBCS6 and DNHBCS18 in PBS media. Both DNHBCS6 and DNHBCS18 exhibited increasing EW trend: acidic (pH 3 – 4) < basic (pH 8 – 9) < neutral. Optimal EW of DNHBCS*x* was observed at neutral pH because COO^- groups remain ionized without excessive ionic interference, thus maximizing electrostatic repulsion and water absorption. In the acidic conditions (pH 3 – 4), EW values of DNHBCS6 and DNHBCS18 were the lowest, at 29.11 g/g and

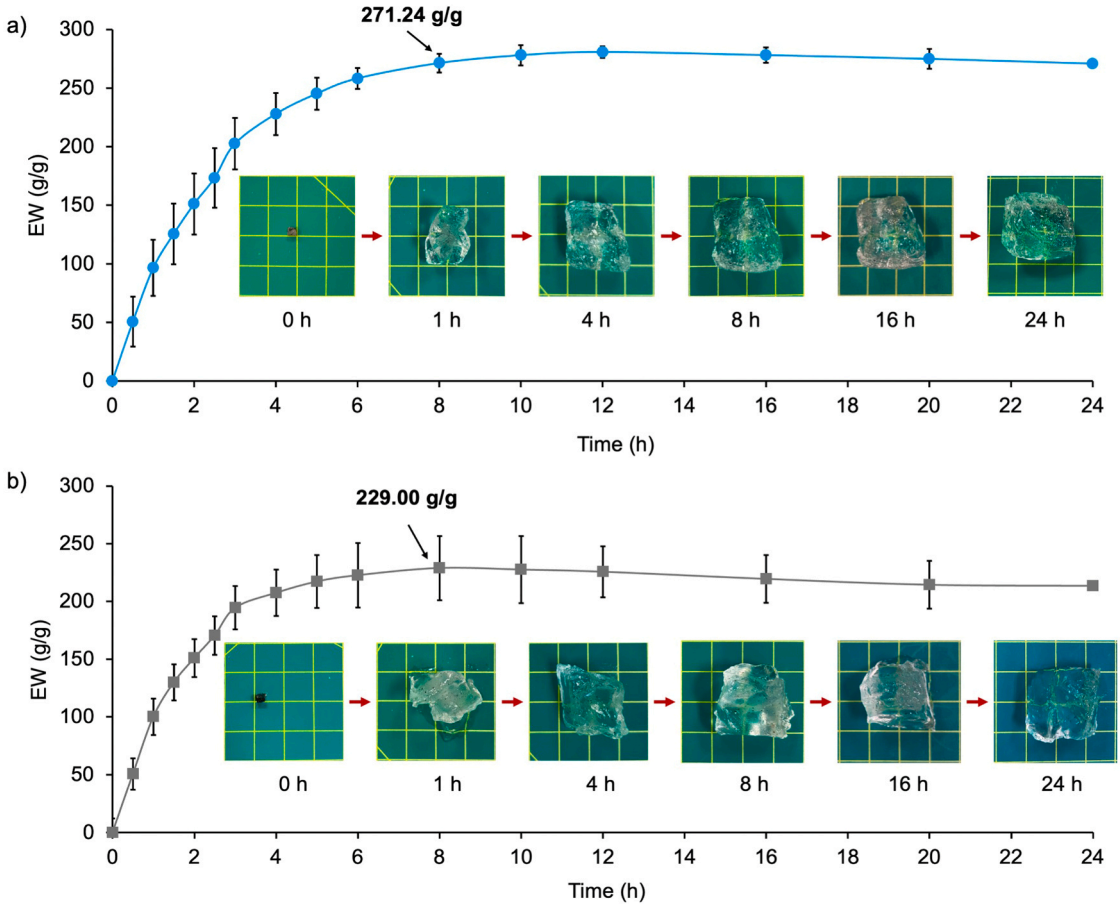

Fig. 6. Time-dependent swelling of (a) DNHBCS6 and (b) DNHBCS18 in DI water, where the photographs (inset) show the evolution of swollen morphologies of respective hydrogel composites.

26.20 g/g, respectively, which was likely due to protonation of carboxylate ions that eliminates anion-anion repulsive effect and enhanced the intermolecular hydrogen bonding between –COOH and -OH moieties, leading to restricted volume expansion in the hydrogel composites. At mildly basic pH (pH 8 – 9), these carboxylic groups deprotonate to form $–COO^-$, creating more electrostatic repulsion that boosts EW of DNHBCS*x* [50,74].

Comparing EW performance in tap water with that of DI water is practically important because irrigation in agriculture typically relies on tap or groundwater rather than purified water. Lower EW in tap water compared to DI water is expected because tap water contains dissolved salts and hardness ions, such as Na^+, Ca^{2+} and Mg^{2+}, which are absent in DI water (Fig. 7b). These ions partially shield the negative charges along the DNHBCS*x*'s polymer backbones, reducing osmotic swelling pressure and polymer chain relaxation. The cations present in tap water can also form ionic bridges between carboxylate groups, creating supplementary crosslinking points that can further restrict pore expansion This observation demonstrates the sensitivity of the DNHBCS*x* composite to dissolved ions. Despite this 11 – 15% EW reduction, the DNHBCS*x* composite maintain substantial water absorbency in tap water between 217.57 g/g and 270.40 g/g, indicating their functional effectiveness under realistic irrigation conditions.

Extending the evaluation of DNHBCS6 to saline environments consisting of multivalent ions at 0.9% w/v, a pronounced decline in EW with increasing cation valence and ionic strength (Fig. 7c), following the order [15,75]:

$$KCl > NaCl > CaCl_2 > > FeCl_3$$

Monovalent ions (Na^+, K^+) primarily reduce swelling through charge screening, leading to moderate EW values. The slightly higher EW in KCl compared to NaCl may arise from weaker ion–polymer interactions and larger hydrated ionic radius. In contrast, Ca^{2+} significantly suppresses swelling through ionic bridging between $–COO^-$ groups [13], forming more crosslinks that reduce mesh size and stiffen the DNHBCS6, leading to extremely low EW (2.62 g/g). The strongest inhibition occurs in the presence of trivalent Fe^{3+} ions (EW < 1 g/g) owing to dense coordination crosslinks that strongly compress the composite matrix and severely restrict water uptake [76,77].

Comparison with DNH highlights the beneficial influence of BC on water absorbency and saline tolerance (Fig. 7b-c). The DNHBCS*x* composites consistently showed higher EW than DNH, demonstrating the role of BC in water uptake. Addition of porous BC increases porosity in the DNHBCS*x* composites and facilitate capillary water storage, thus improving water transport pathways within the composite network. This cation-sensitive swelling behaviour across PBS media of varying pH, tap water and saline solutions demonstrates that water uptake of DNHBCS*x* is controlled by charge screening, osmotic pressure reduction and ionic crosslinking effects, typical of poly(acrylate) hydrogels [13,15,75]. Moreover, the dissolved ions can compete with the ionic moieties within DNHBCS*x* for water molecules, limiting the hydrogel's expansion [78]. Importantly, DNHBCS*x* retains measurable swelling in saline environments, indicating functional water retention capacity in saline conditions.

Figures S8 illustrates the dimensional changes of cylindrical DNHBCS6 and DNH samples during immersion in DI water and saline solutions, followed by subsequent re-immersion of the salt-loaded cylinders in DI water. Corresponding EW and volume expansion data are shown in Figure S9. A detailed discussion is available in Supporting

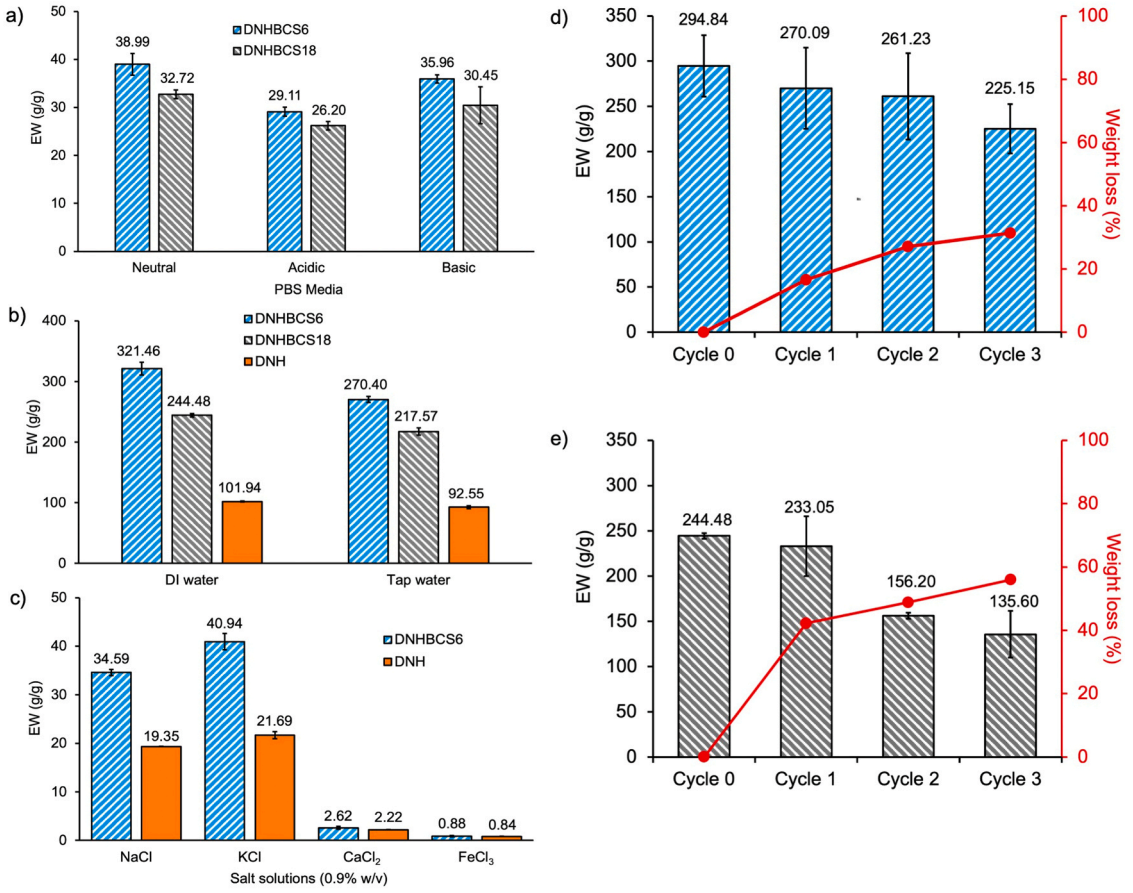

Fig. 7. Water absorbency (EW) of DNHBCS*x* under different aqueous environments: (a) PBS media at different pH conditions; (b) DI water versus tap water; and (c) saline solutions containing different cations (0.9% w/v NaCl, KCl, $CaCl_2$ and $FeCl_3$). Reswellability in DI water for (d) DNHBCS6 and (e) DNHBCS18. The weight losses (%) of DNHBCS*x* (red-coloured lines) for each cycle are presented on the secondary y-axis (red colour).

Information S7. Both hydrogels exhibited the enhanced structural stability and shape recovery characteristic of double network hydrogels, with DNHBCS6 samples exhibited more controlled volume expansion but markedly higher EW (Figure S8, Figure S9a-b) than those of DNH control (Figure S9c-d) across varying ionic environments. All cylindrical hydrogels exposed to multivalent cation solutions showed gradual volume recovery upon re-immersion in DI water, confirming reversible ionic interactions and preserved network connectivity. Dimensional recovery was most complete after monovalent salt exposure and remained appreciable after Ca^{2+} treatment. Reversible swelling after NaCl and $CaCl_2$ exposure is agronomically important because real soils and irrigation waters commonly contain Na^+ and Ca^{2+} [13]. The ability of DNHBCS6 to recover from Na^+ and Ca^{2+} induced contraction enables restoration of water retention performance after rainfall or fresh water irrigation, and supports continued functionality as a WRA in salt-affected and calcareous soils under fluctuating field conditions.

3.8. Reswellability dan durability

The reswellability of hydrogel composites determines their long-term performance in agricultural fields. Hydrogel composites exhibiting high EW and reswelling efficiency are highly desired as they can maintain soil moisture better over extended periods to support plant growth during intermittent drought conditions whilst reducing irrigation frequency. Therefore, evaluating the reswellability of DNHBCS*x* is essential, as it directly influences the optimization of irrigation scheduling and water resource management when it is applied in the field.

Reswellability and structural durability (material weight loss) of the DNHBCS*x* composites in DI water over consecutive wetting-drying cycles is presented in Fig. 7d-e. A progressive decline in EW was observed with increasing wetting-drying cycles, indicating reduced swelling capacity upon repeated use. The first bar denotes EW during initial swelling (Cycle 0), while subsequent bars represent reswelling capacity after each wetting–drying cycle (Cycle 1–3). The EW of DNHBCS6 decreased gradually from an initial EW of 294.84 g/g to 270.09 g/g after Cycle 1, and continued to decline progressively to 225.15 g/g (Cycle 3) as shown in Fig. 7d. In contrast, a more pronounced EW decrease was seen in DNHBCS18 (Fig. 7e), decreasing from an initial EW of 244.48 g/g to 233.05 g/g (Cycle 1), and further reducing to 135.60 g/g in Cycle 3. For comparison, DNH showed consistent reswellability with substantially lower EW values compared to DNHBCSx composites across similar wetting–drying experiment. After Cycle 3, the EW for DNH stabilized within a narrow range of 95.40 g/g and 104.98 (Figure S10). The slight EW increase after Cycle 0 is likely attributed to improved water accessibility after initial swelling as polymer chains relax and rearrange. These results highlight the role of double network matrix in resisting network rupture and enhancing the structural stability of both DNHBCSx and DNH during repeated hydration–dehydration cycles.

The superior EW performance and reswellability of DNHBCS6 compared to DNHBCS18 can be attributed to differences in their compositional balance and network architecture. The water absorption performance and reswellability of these double network hydrogel composites were strongly influenced by the relative proportions of covalently-crosslinked P(AA-*co*-AM), physically-crosslinked PVA and BC loading. The covalently-crosslinked P(AA-*co*-AM) network served as the primary water-absorbing framework in the superabsorbent DNHBCS*x*. Although the higher MBA concertation did not directly enhance the EW

performance, the increased crosslinked density provided the essential structural stabilization to the DNHBCS6's architecture. Increasing PVA fraction might have reinforced the bulk rigidity and elasticity of DNHBS18, but its crystalline hydrogen-bonded domains restricted water penetration and substantially reduced the EW performance. Conversely, the higher BC loading in DNHBCS6 not only acted as reinforcing filler to the polymeric matrix, but also as the oxygen-rich hydrophilic component that enhanced its rapid water uptake during repeated swelling–-drying with minimal weight loss, showcasing the robustness of DNHBCS6.

The DNHBCS*x* composites and DNH are polymeric materials consisting of water soluble synthetic polymers P(AA-*co*-AM) and PVA, which are generally regarded as low-toxicity and environmentally safe [79]. Nevertheless, evaluating their durability under the cyclic hydration-dehydration conditions remain important, given the ongoing concerns being regarding microplastic persistence and residual monomers. After three consecutive cycles of wetting-drying, the cumulative weight losses of spent DNHBCS6 and DNHBCS18 reached 31.31% and 55.96%, respectively, relative to their initial weights (Fig. 7d-e). Interestingly, DNHBCS6 was able to sustain high EW (> 200 g/g) with significantly lower weight loss compared to DNHBCS18. The observed weight loss in the more porous DNHBCS*x* structure is attributed primarily to the leaching of loosely bound polymer fractions, weakly entrapped biochar particles and K^+ ions when the polymer network relaxes during repeated hydration cycles, reflecting physical deterioration of the composites rather than chemical backbone degradation [15, 80]. Comparatively, DNH exhibited only 14.36% weight loss after Cycle 3 (Figure S10), approximately two-fold lower than that of the DNHBCS*x* composites. This lower weight loss can be attributed to the denser and less porous structure of the pristine DNH, which limits the loss of water-soluble K^+ and other small molecules during cyclic hydration.

Fig. 8 depicts the dimensional and structural evolution of cylindrical hydrogels prepared in the as-synthesized state, followed by oven drying and reswelling in DI water over two wetting–drying cycles. Both DNHBCS6 and DNH expanded substantially upon hydration, forming cohesive swollen cylindrical hydrogels. DNHBCS6 consistently exhibited higher EW and retained clearer shape definition with smoother edges, indicating stronger network integrity during initial volumetric expansion. After oven drying, these hydrogels contracted substantially. Upon the first reswelling, DNHBCS6 recovered its original cylindrical geometry despite decreased volume expansion, demonstrating good shape memory and network elasticity. In contrast, DNH exhibited much lower EW with similar volume expansion, accompanied by surface wrinkling and minor fragmentation.

Their structural differences become more pronounced after the second wetting–drying cycle. While DNHBCS6 cylinder remained intact with moderate dimensional reduction, DNH cylinder underwent progressive fragmentation and network deterioration. In the absence of BC filler, the DNH exhibited cumulative structural damage during cyclic hydration, consistent with limited stress-dissipation and reinforcement. By contrast, the more structurally intact DNHBCS6 support the synergistic role of BC as the reinforcing filler within the double network matrix enhancing structural integrity and improved resistance to cyclic structural fatigue while preserving water absorption functionality. The more controlled volume expansion of DNHBCS6 during cyclic hydration–dehydration further corroborates the observations in Figures S8 – S9, despite minor batch-to-batch variations in EW values. Such moderated swelling is advantageous for soil applications, as it helps maintain pore connectivity and reduces the risk of soil pore clogging, thereby sustaining aeration and water infiltration.

3.9. Water holding and water retention capacities in soils

The performance of DNHBCS6 as WRA was evaluated in sandy loam and clay loam soils, where DNHBCS6 was mixed thoroughly with the soil and incubated for 31 days (Fig. 9a). Addition of 2 wt% DNHBCS6 increased WHC in both soil textures compared to the untreated controls. In sandy loam, WHC increased by ~50%, from 81.47% (control sandy loam) to 121.47% (DNHBCS6). A similar trend was observed in clay loam, where higher WHC was observed in clay loam amended with DNHBCS6 (149.49%), compared to control (103.64%). In both soils, DNHBCS6 outperformed DNH slightly (115.1% in sandy loam; 142.23%

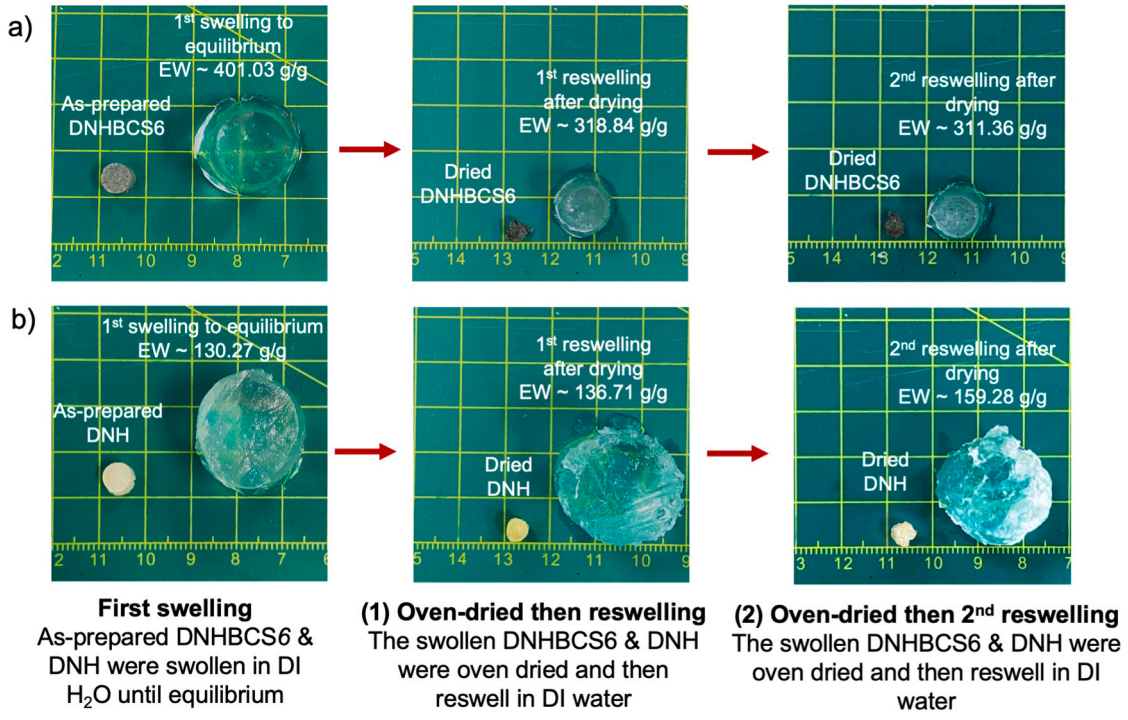

Fig. 8. Photographs comparing the dimensional and structural evolution of as-prepared (a) DNHBCS6 and (b) DNH cylindrical hydrogels followed by oven drying and reswelling in DI water over two wetting–drying cycles.

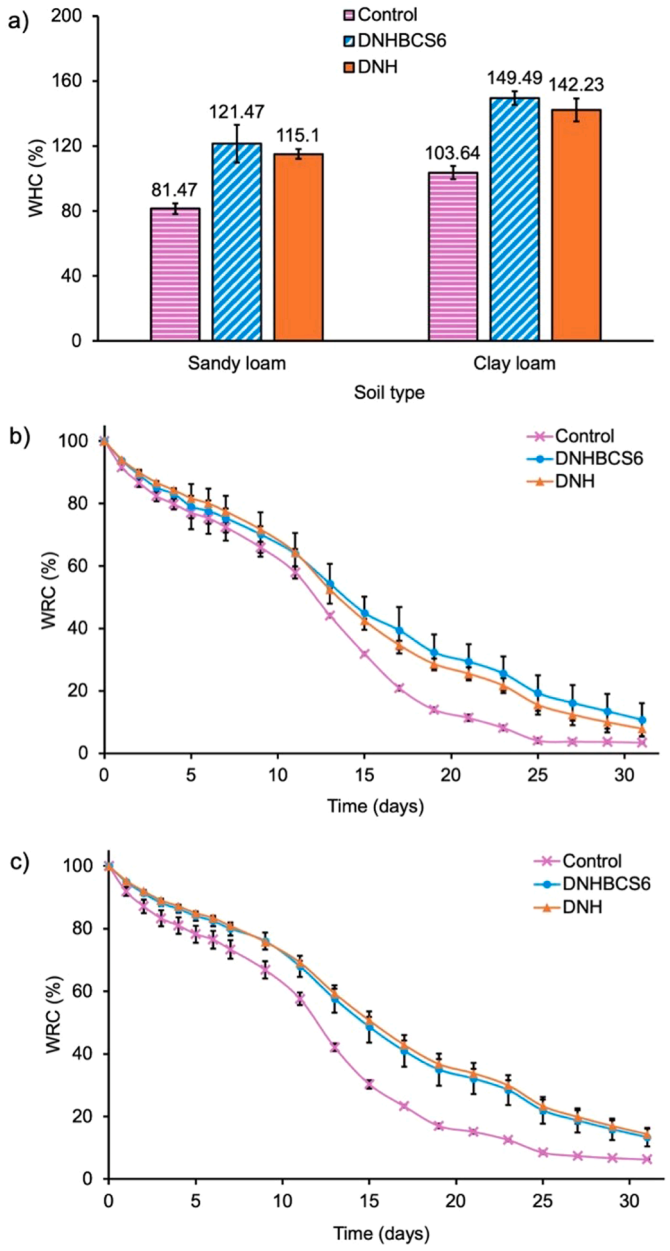

Fig. 9. (a) WHC in sandy loam and clay loam of DHNBCS6 and DNH. WRC of DHNBCS6 and DNH in (b) sandy loam and (c) clay loam.

in clay loam), which suggests that BC in DNHBCS6 composite provide additional water holding benefit beyond the hydrogel.

The WRC experiments were normalized by starting at ~100% WHC in each soil, ensuring that subsequent differences reflect water-loss kinetics due to drying rather than different initial moisture contents. The control soils demonstrated faster decline after 10 – 15 incubation days in both tested soil textures (Fig. 9b-c). After 15 days of evaporation, the separation between DNHBCS6 and DNH curves becomes more apparent in sandy loam (Fig. 9b). DNHBCS6 retained more than twice as much water (29.33%) as the control (11.33%) at Day 21, and remained ~4% higher than DNH until the end of the experiment, with WRC of 10.75% (DNHBCS6) and 7.89% (DNH) compared to only 3.44% in control sandy loam. In the presence of BC, DNHBCS6 not only increases the total water retained in sandy loam, but also slows down moisture loss possibly by trapping water within additional capillary storage sites and microchannels of BC embedded in the more porous DNHBCS6 composite.

However, DNHBCS6 and DNH showed comparable water retention behaviour in clay loam with nearly overlapping WRC profiles and ended with WRC of 13.39% and 14.31% after 31 days, while control clay loam was observed at 6.29% (Fig. 9c). This implies that the high intrinsic water-retention capacity of the fine-textured clay loam governs moisture loss, while the hydrogel WRAs mainly serve as supplementary water storage that enhance water availability without modifying the soil's intrinsic water retention properties.

3.10. Performance comparison with other WRAs

Table 5 compares the water absorption performance of our optimized DNHBCS*x* hydrogel composite against other WRAs, including hydrogel-only systems, other hydrogel-biochar composites and commercial SAHs. Water absorbency data for isolated biochar used solely as "absorbent" material is limited because biochar does not swell like hydrogels. However, most studies evaluated biochar for its ability in enhancing soil water holding capacity, an effect primarily stems from increased porosity and pore connectivity rather than direct water absorption.

Agronomic effectiveness depends not only on maximum absorbency but also on structural stability, resistance to excessive swelling that may clog soil pores, water retention under load and structural durability during repeated wetting–drying cycles. As shown in Table 5, the optimized DNHBCS6 containing 3% w/v BC demonstrated maximum water absorbency of 328.28 g/g in DI water and good tolerance in saline condition (34.59 g/g in 0.9% w/v NaCl and 40.94 g/g in 0.9% w/v KCl), positioning it between commercial SAPs and other hydrogel-biochar composites. Its EW performance was greater than biopolymer-based hydrogels, such as cellulose hydrogels [81] and within the range of other engineered hydrogels [82]. When compared with other hydrogel-biochar composites, despite not reaching the extremely high absorbency of CMC-hydrogel–rice husk biochar composites (3240 g/g) [23] or magnesium–corn straw biochar hydrogels (1395 g/g) [31], its water absorbency performance was comparable to, and in some cases exceeded, the values reported in previous studies involving single-network or semi-IPN systems [5,22,29,83]. It demonstrated superior multicyclic resilience whilst retaining EW of 225 g/g, setting it apart from most reported hydrogel-biochar composites that often lacks such cyclic stability data. Furthermore, SAHs with ultra-high swelling often become mechanically weak and lose integrity under soil confinement, a limitation seldom discussed in the literature.

The DNHBC design prioritizes functional stability over maximum EW or swelling. DNHBCS6 offers a competitive balance comprising of moderate-to-high water absorbency even after repetitive use owing to the structural durability of the double network composite and saline tolerance. The composite also exhibited reversible swelling after Na^+ and Ca^{2+} exposure with minimal structural disintegration. This enables restoration of water retention capacity after rainfall or irrigation to support continued functionality in salt-affected and calcareous soils. This performance effectively addresses the key limitations of existing hydrogel-only and hydrogel-biochar matrices. Based on shape recovery after rewetting and resistance of structural fatigue, the observed cumulative weight loss of 31% after three wetting-drying cycles is likely attributed to partial network deterioration (< 15% in pristine DNH) and the leaching of weakly bound biochar particles and K^+ ion. Importantly, these released components may beneficially enhance soil structure and porosity while supplying exchangeable K^+, thereby supporting soil fertility and moisture retention.

DNHBCS6 effectively bridges the gap between fully synthetic and biomass-derived hydrogels, integrating the structural durability and functionality of synthetic polymers with environmental compatibility associated with biochar. The one-pot aqueous polymerization of DNHBCS6 under mild conditions (≤70°C) using readily available raw materials offers a scalable and cost-effective synthetic route. In addition to enhancing structural integrity and water absorbency, the incorporation of 3% w/v BC reduces the overall polymer content by 10 – 15%,

Table 5
Comparison of water absorbency performance of hydrogel-only, hydrogel-biochar and commercial SAHs.

Type of soil conditioner	Formulation	Maximum water absorbency (distilled or DI water)	Water absorbency (saline environment)	Reference
Hydrogel only	Cellulose hydrogels + sodium carboxy-methylcellulose (NaCMC, 1.75%), glycerol (1%) and polyethylene glycol (PEG, 0.5%) separately	~ 26 g/g (2600%)	N/A	[81]
	Carboxymethyl cellulose-g-(polyacrylamide-co-2-acrylamido-2-methylpropanesulfonic acid), {CMC-g-(PAM-co-PAMPS)}	313 g/g	N/A	[82]
	2-pyridyl) acetyl chitosan chloride-g-poly(acrylic acid-*co*-acrylamide), {PACS/P(AA-*co*-AM)}	615 g/g Maintained > 50% water absorbency after 5× swelling	44 g/g in 0.9% w/v NaCl	[84]
Hydrogel-biochar composite	Carboxymethyl cellulose hydrogel + 0.1 g rice husk biochar,{CMC-H-B}	3240.07 g/g	220–240 g/g in 0.15 M (~0.9% w/v) NaCl	[23]
	Acrylamide/sodium carboxymethyl cellulose/modified peanut shell biochar, {AM/CMC/MB}	33.83 g/g	N/A	[83]
	Soy protein–based hydrogel+ 4% bamboo biochar, {SPB}	222.3 – 340 g/g independent of pH	N/A	[22]
	Cellulose-yellow pine wood biochar, {BH1.0}	9.023 g/g (902.3%) within 30 h	N/A	[29]
	Vine pruning waste-derived biochar BC + polyvinyl alcohol (PVA) + sodium alginate (SA)	3.52 g/g (352%)	5.49 g/g (549%) in 1% NaCl	[5]
	Magnesium-corn straw biochar modified polyacrylate, {Mg-NBC/PAA}	1395.12 g/g	N/A	[31]
	DNHBCS6	321.46 g/g; 225.15 g/g after 3 wetting-drying cycles	35–41 g/g in 0.9% w/v NaCl and KCl 29 – 39 g/g in PBS, pH 3–9 Reversible swelling for Na^+ and Ca^{2+}-loaded DNHBCS6	This study
Other hydrogel composite	Semi-IPN starch-graft-poly(acrylic acid-*co*-acrylamide)/polyvinyl alcohol/clinoptilolite	364.82 g/g	46 g/g	[85]
Commercial SAH	Hydrostock (94% potassium polyacrylate) from Vestigo Ventures, Malaysia	441.2 g/g	~50 g/g in 0.9% w/v NaCl	[23]
	STOCKOSORB® 660 (potassium polyacrylate) by Evonik Industries, Germany	250 g/g	100 g/g in 0.1% NaCl	[86]
	AQUASORB B3005 (polyacrylamide–acrylic acid salt copolymer) by SNF Inc., Riceboro, Georgia, USA	300 g/g	150 g/g in 0.1% NaCl	[86]

Note: Not available (N/A

improving economic feasibility and competitiveness with commercial SAPs (USD 1.00–4.50 per kg, depending on grade and volume). Controlled swelling, cyclic resilience and salt-responsive reversibility enable sustained soil moisture retention without excessive volume expansion that could impair soil aeration, highlighting its potential as a multifunctional WRA for sustainable agricultural applications, particularly in coarse-textured soils.

Despite its promising performance, several limitations require further investigation. The current study is based on laboratory-scale evaluations, therefore field-scale validation is recommended to assess soil-specific application rates, crop response and long-term soil-polymer interactions to ensure the DNHBCS6's viability as a sustainable WRA with soil conditioning benefits. The material weight loss observed during cyclic wetting–drying suggests partial network degradation and biochar leaching, which may influence long-term durability and performance consistency. Future work should include comprehensive cost

Table 6
Comparison of DNHBCS6 with commercial synthetic SAHs and biopolymer-based SAHs across cost efficiency, performance and environmental sustainability as WRAs.

Category	DNHBCS*x* Composite	Synthetic SAHs	Biopolymer-based SAHs
Cost efficiency			
Raw materials	Moderate; polymer partially replaced by low-cost PKS biochar	Moderate–high; petroleum-derived polymers	Low–moderate; renewable biomass feedstocks [72]
Replacement frequency	Lower, due to reinforced double network structure	Low-moderate	Higher, due to biodegradation [12,76]
Lifecycle cost outlook	Potential lifecycle cost savings	Established but recurring cost	Low upfront cost but increases with reapplication [76]
WRA Performance			
Water absorption capacity	Intermediate-high; internal storage via porous composite structure [76]	Very high in DI water [87]	Low-moderate [88]
Soil water retention	Moderate moisture buffering and gradual release	High but may release water rapidly [87]	Moderate; influenced by degradation [88]
Salinity sensitivity	Low-moderate, enhanced ionic tolerance	Moderate (acrylamide-based)-high (acrylate-based) [87]	Inconsistent behaviour and sensitive to environmental variables (pH and temperature) [88]
Structural durability	Reinforced by PKS BC filler and double network, with controlled swelling behaviour [76]	Moderate - high, uncontrolled swelling (typically single-network or semi-IPN) [76]	Low–moderate (typically single-network or semi-IPN) [10]
Wet–dry cycle stability	Enhanced cyclic stability	Moderate	Limited information
Soil compatibility	Improves pore connectivity and moisture distribution	Neutral	Biocompatible but less durable [12]
Environmental impact			
Polymer loss risk	Potential reduction due to improved integrity	Potential microplastic persistence, slow degradation [77,89]	Biodegradable with minimal residues [12]
Carbon footprint	Potential reduction; PKS biochar contributes to carbon sequestration	No sequestration benefit	Low carbon footprint, biodegradation leads to carbon sequestration [76]
Sustainability	Balanced durability and environmental benefit	Effective but environmental concerns	Sustainable but less durable [12,87]

evaluation, supported by life cycle assessment (LCA) and techno-economic analysis (TEA), to confirm large-scale feasibility and environmental sustainability. Further development of nutrient-loading functionality is recommended to advance the material toward controlled-release fertilizer applications. Table 6 compares DNHBCS6 composite against commercial synthetic and biopolymer-based SAHs with respect to cost efficiency, performance and environmental sustainability to contextualize its practical relevance.

4. Conclusion

Novel double network hydrogel-biochar composites (DNHBCS*x*) were successfully synthesized via a facile one-pot approach. Response Surface Methodology–Central Composite Design (RSM-CCD) optimization identified PVA and biochar (BC) loadings as the most influential parameters governing water absorbency (EW). The optimized formulations, DNHBCS6 and DNHBCS18 (1–2% w/v PVA; 2–3% w/v BC), achieved competitive EW, buffered pH responsiveness and enhanced structural integrity under saline conditions compared to pristine DNH, despite the expected order-of-magnitude reduction in swelling at high ionic strength. Recovery of water retention capacity of DNHBCS6 following NaCl- and CaCl-induced contraction indicates reversible swelling, an agronomically relevant feature for soils and irrigation waters containing Na^{+} and Ca^{2+}. DNHBCS6 maintained high EW > 220 g g^{-1} after three wetting–drying cycles despite 31% weight loss, demonstrating the synergistic reinforcement provided by BC, which improves resistance to cyclic structural fatigue without compromising water-absorption performance. Of particular importance, the controlled swelling behaviour of DNHBCS6 enables high water absorbency while minimizing excessive volume expansion, helping maintain soil pore connectivity and reduce pore clogging for sustained aeration under field conditions. The balanced composition of DNHBCS6, combining sufficient crosslink density and PVA content for network elasticity and shape memory with high BC filler loading for structural reinforcement, porosity and hydrophilicity, produced a fast-absorbing, structurally resilient and salt-tolerant superabsorbent composite. Collectively, these features establish DNHBCS6 as a robust WRA material with strong potential for sustainable agriculture, particularly in saline or drought-prone environments, and as a promising platform for future controlled-release applications.

CRediT authorship contribution statement

Dzureen Julaihi: Methodology, Investigation, Formal analysis, Data curation, Visualization, Writing – original draft. **Cindy Soo Yun Tan:** Funding acquisition, Project administration, Conceptualization, Methodology, Supervision, Visualization, Formal analysis, Data curation, Writing – original draft, Writing – review & editing. **Lin-Chi Wang:** Resources, Investigation, Writing – review & editing. **Mohamad Izzat Arif Nordin:** Methodology, Investigation. **Kavirajaa Pandian Sambasevam:** Supervision, Methodology, Formal analysis, Writing – review & editing. **Suk-Fun Chin:** Supervision, Resources, Writing – review & editing. **Fui Kiew Liew:** Investigation, Writing – review & editing. **Su Shiung Lam:** Resources, Writing – review & editing. **Peter Nai Yuh Yek:** Resources, Methodology. **Margaret Abat:** Resources, Writing – review & editing. **Nazrizawati Ahmad Tajuddin:** Writing – review & editing.

Declaration of Competing Interest

The authors declare that they have no known competing financial interests or personal relationships that could have appeared to influence the work reported in this paper.

Acknowledgements

This project was supported by the Ministry of Higher Education, Malaysia through the Fundamental Research Grant Scheme (Grant number: FRGS/1/2023/STG04/UITM/02/9) and Universiti Teknologi MARA. The authors also acknowledged Latonia Nur Adyanis (National Kaohsiung University of Science and Technology, Taiwan) for the SEM analyses and Nur Ellydia Mohamad Gustie Noorambia (Universiti Teknologi MARA) for her assistance in the project.

Appendix A. Supporting information

Supplementary data associated with this article can be found in the online version at doi:10.1016/j.jece.2026.122337.

Data availability

Data will be made available on request.

References

[1] H. Mansouri, H. Ait Said, H. Noukrati, A. Oukarroum, H. Ben youcef, F. Perreault, Advances in controlled release fertilizers: Cost-effective coating techniques and smart stimuli-responsive hydrogels, Adv. Sustain. Syst. 7 (9) (2023) 2300149, https://doi.org/10.1002/adsu.202300149.
[2] C. He, Z. Liu, J. Wu, X. Pan, Z. Fang, J. Li, B.A. Bryan, Future global urban water scarcity and potential solutions, Nat. Commun. 12 (1) (2021) 4667, https://doi.org/10.1038/s41467-021-25026-3.
[3] P. Mehta, S. Siebert, M. Kummu, Q. Deng, T. Ali, L. Marston, W. Xie, K.F. Davis, Half of twenty-first century global irrigation expansion has been in water-stressed regions, Nat. Water 2 (3) (2024) 254–261, https://doi.org/10.1038/s44221-024-00206-9.
[4] J. Park, W. Guan, C. Lei, G. Yu, Self-irrigation and slow-release fertilizer hydrogels for sustainable agriculture, ACS Mater. Lett. 6 (8) (2024) 3471–3477, https://doi.org/10.1021/acsmaterialslett.4c01120.
[5] Y. Uysal, Z.G. Doğaroğlu, M.N. Makas, Z. Çaylali, Boosting Water Retention in Agriculture: Vine Biochar-Doped Hydrogels' Swelling and Germination Effects, Glob. Chall. 8 (5) (2024) 2300254, https://doi.org/10.1002/gch2.202300254.
[6] Y. Xu, Y. Gao, W. Li, S. Chen, Y. Li, Y. Shi, Effects of compound water retention agent on soil nutrients and soil microbial diversity of winter wheat in saline-alkali land, Chem. Biol. Technol. Agric. 10 (1) (2023) 2, https://doi.org/10.1186/s40538-022-00375-3.
[7] J. Zhu, Z. Zhang, Y. Wen, X. Song, W.K. Tan, C.N. Ong, J. Li, Recent advances in superabsorbent hydrogels derived from agro waste materials for sustainable agriculture: A review, J. Agric. Food Chem. 72 (41) (2024) 22399–22419, https://doi.org/10.1021/acs.jafc.4c04970.
[8] Y. Liu, J. Wang, H. Chen, D. Cheng, Environmentally friendly hydrogel: A review of classification, preparation and application in agriculture, Sci. Total Environ. 846 (2022) 157303, https://doi.org/10.1016/j.scitotenv.2022.157303.
[9] D. Skrzypczak, K. Mikula, N. Kossińska, B. Widera, J. Warchoł, K. Moustakas, K. Chojnacka, A. Witek-Krowiak, Biodegradable hydrogel materials for water storage in agriculture - review of recent research, Desalin. Water Treat. 194 (2020) 324–332, https://doi.org/10.5004/dwt.2020.25436.
[10] A. Ali, S. Ahmed, Recent advances in edible polymer based hydrogels as a sustainable alternative to conventional polymers, J. Agric. Food Chem. 66 (27) (2018) 6940–6967, https://doi.org/10.1021/acs.jafc.8b01052.
[11] A. El Idrissi, B.-e Channab, Y. Essamlali, M. Zahouily, Superabsorbent hydrogels based on natural polysaccharides: Classification, synthesis, physicochemical properties, and agronomic efficacy under abiotic stress conditions: A review, Int. J. Biol. Macromol. 258 (2024) 128909, https://doi.org/10.1016/j.ijbiomac.2023.128909.
[12] H. Xue, P. Wang, L. Ji, K. Zhang, S. Ge, J. Tan, Polysaccharide-based hydrogels: Materials, preparation, and applications in medicine, food, adsorption, and agriculture, J. Agric. Food Res. (2025) 102395, https://doi.org/10.1016/j.jafr.2025.102395.
[13] J. Liang, Y. Yan, L. Chen, J. Wu, Y. Li, Z. Zhao, L. Li, Synthesis of carboxymethyl cellulose-g-poly(acrylic acid-co-acrylamide)/polyvinyl alcohol sponge as a fast absorbent composite and its application in coral sand soil, Int. J. Biol. Macromol. 242 (2023) 124965, https://doi.org/10.1016/j.ijbiomac.2023.124965.
[14] M. Salimi, E. Motamedi, B. Motesharezedeh, H.M. Hosseini, H.A. Alikhani, Starch-g-poly(acrylic acid-co-acrylamide) composites reinforced with natural char nanoparticles toward environmentally benign slow-release urea fertilizers, J. Environ. Chem. Eng. 8 (3) (2020) 103765, https://doi.org/10.1016/j.jece.2020.103765.
[15] W. Tanan, J. Panichpakdee, S. Saengsuwan, Novel biodegradable hydrogel based on natural polymers: Synthesis, characterization, swelling/reswelling and biodegradability, Eur. Polym. J. 112 (2019) 678–687, https://doi.org/10.1016/j.eurpolymj.2018.10.033.
[16] Q. Zhang, G. Yu, Q. Zhou, J. Li, Y. Feng, L. Wang, Y. Tang, Y. Peng, Eco-friendly interpenetrating network hydrogels integrated with natural soil colloid as a green

and sustainable modifier for slow release of agrochemicals, J. Clean. Prod. 269 (2020) 122060, https://doi.org/10.1016/j.jclepro.2020.122060.
[17] X. An, Z. Wu, J. Yu, G. Cravotto, X. Liu, Q. Li, B. Yu, Copyrolysis of biomass, bentonite, and nutrients as a new strategy for the synthesis of improved biochar-based slow-release fertilizers, ACS Sustain. Chem. Eng. 8 (8) (2020) 3181–3190, https://doi.org/10.1021/acssuschemeng.9b06483.
[18] D.H.H. Sim, I.A.W. Tan, L.L.P. Lim, B.H. Hameed, Encapsulated biochar-based sustained release fertilizer for precision agriculture: A review, J. Clean. Prod. 303 (2021) 127018, https://doi.org/10.1016/j.jclepro.2021.127018.
[19] Q. Duan, S. Jiang, F. Chen, Z. Li, L. Ma, Y. Song, X. Yu, Y. Chen, H. Liu, L. Yu, Fabrication, evaluation methodologies and models of slow-release fertilizers: A review, Ind. Crops Prod. 192 (2023) 116075, https://doi.org/10.1016/j.indcrop.2022.116075.
[20] W. Shi, Y. Ju, R. Bian, L. Li, S. Joseph, D.R. Mitchell, P. Munroe, S. Taherymoosavi, G. Pan, Biochar bound urea boosts plant growth and reduces nitrogen leaching, Sci. Total Environ. 701 (2020) 134424, https://doi.org/10.1016/j.scitotenv.2019.134424.
[21] W. Wei, Z. Zhang, M. Wu, X. Zhang, T. Zhang, Z. Wang, G. Li, The preparation of starch-based green adsorption gel with tunable water channels through extrusion-dual cross-linking method, Int. J. Biol. Macromol. 304 (2025) 140818, https://doi.org/10.1016/j.ijbiomac.2025.140818.
[22] J. Liang, Z. Zhao, M. Xing, X. Wang, Y. Dong, Y. Yang, N. Du, H. Gu, L. Meng, W. Peng, C. Li, Improving properties of soy protein–based hydrogel composites by incorporating bamboo biochar towards slow release and water retention of fertilizers and enhanced plant growth, Adv. Compos. Hybrid. Mater. 8 (1) (2025) 53, https://doi.org/10.1007/s42114-024-01114-y.
[23] J. Ye, R. Abdullah, T.C. Ling, Synthesis of carboxymethyl cellulose-based superabsorbent hydrogel-biochar composite as an eco-friendly water retention agent for soil moisture management, Int. J. Biol. Macromol. (2025) 146593, https://doi.org/10.1016/j.ijbiomac.2025.146593.
[24] T.A.T. Yasim-Anuar, L.N. Yee-Foong, A.A. Lawal, M.A.A. Farid, M.Z.M. Yusuf, M. A. Hassan, H. Ariffin, Emerging application of biochar as a renewable and superior filler in polymer composites, RSC Adv. 12 (22) (2022) 13938–13949, https://doi.org/10.1039/D2RA01897G.
[25] S. Chen, M. Yang, C. Ba, S. Yu, Y. Jiang, H. Zou, Y. Zhang, Preparation and characterization of slow-release fertilizer encapsulated by biochar-based waterborne copolymers, Sci. Total Environ. 615 (2018) 431–437, https://doi.org/10.1016/j.scitotenv.2017.09.209.
[26] M.R. Zakaria, M.A.A. Farid, Y. Andou, I. Ramli, M.A. Hassan, Production of biochar and activated carbon from oil palm biomass: current status, prospects, and challenges, Ind. Crops Prod. 199 (2023) 116767, https://doi.org/10.1016/j.indcrop.2023.116767.
[27] P. Singh, A. Pathy, S. Sharma, M. Dhanorkar, M.A. Naeth, S.X. Chang, Expanding the frontiers of nanobiochar and biochar nanocomposites as versatile biomaterials for sustainable development, Biochar 8 (1) (2026) 15, https://doi.org/10.1007/s42773-025-00523-6.
[28] S.K. Das, G.K. Ghosh, Hydrogel-biochar composite for agricultural applications and controlled release fertilizer: A step towards pollution free environment, Energy 242 (2022) 122977, https://doi.org/10.1016/j.energy.2021.122977.
[29] K. Ketheeswaran, S. Shetranjiwalla, M. Krishnapillai, L. Galagedara, Incorporating biochar to make hydrogel composites with improved structural properties, valorized from waste-paper mill sludge and forestry residues using energy efficient protocols, RSC Sustain 2 (11) (2024) 3478–3489, https://doi.org/10.1039/D4SU00332B.
[30] M.I. Rafique, M.I. Al-Wabel, A.S.F. Al-Farraj, M. Ahmad, T. Aouak, H.A. Al-Swadi, M.A. Mousa, Incorporation of biochar and semi-interpenetrating biopolymer to synthesize new slow release fertilizers and their impact on soil moisture and nutrients availability, Sci. Rep. 15 (1) (2025) 9563, https://doi.org/10.1038/s41598-025-90367-8.
[31] Z. Lang, S. Yan, Q. Zhu, Water retention and sustained release of magnesium-based biochar modified hydrogel composite materials, J. Environ. Chem. Eng. 11 (6) (2023) 111380, https://doi.org/10.1016/j.jece.2023.111380.
[32] Z. Zhu, A. Sawut, R. Simayi, X. Jiao, Preparation of hypromellose-graft-polyacrylic acid superabsorbent resin by ultraviolet polymerization and its slow-release performance, ACS Appl. Polym. Mater. 6 (6) (2024) 3128–3138, https://doi.org/10.1021/acsapm.3c02872.
[33] A. Reza, L. Chen, X. Mao, Response surface methodology for process optimization in livestock wastewater treatment: A review, Heliyon 10 (9) (2024), https://doi.org/10.1016/j.heliyon.2024.e30326.
[34] J. Nath, S. Kumar, V. Kumar, Response surface methodology-based modeling and optimization of fenugreek gum-based hydrogel for efficient removal of malachite green dye, J. Mol. Struct. 1293 (2023) 136234, https://doi.org/10.1016/j.molstruc.2023.136234.
[35] M. Paswan, V. Prajapati, B.Z. Dholakiya, Optimization of biodegradable cross-linked guar-gum-PLA superabsorbent hydrogel formation employing response surface methodology, Int. J. Biol. Macromol. 223 (2022) 652–662, https://doi.org/10.1016/j.ijbiomac.2022.11.020.
[36] B.S. Kaith, R. Sharma, S. Kalia, M.S. Bhatti, Response surface methodology and optimized synthesis of guar gum-based hydrogels with enhanced swelling capacity, RSC Adv. 4 (76) (2014) 40339–40344, https://doi.org/10.1039/C4RA05300A.
[37] S.M. Elsaeed, E.G. Zaki, A. Abdelhafes, A.S. Al-Hussaini, Response surface method based modeling and optimization of CMC-g Terpolymer interpenetrating network/bentonite superabsorbent composite for enhancing water retention, ACS Omega 7 (10) (2022) 8219–8228, https://doi.org/10.1021/acsomega.1c03194.
[38] Y. Li, Y. Ma, Y. Wang, F. Chang, J. Dai, Optimization of the Process for Slow-Release Urea Fertilizer with Water Absorption Based on Response Surface Methodology, Appl. Sci. (2024).
[39] J.P. Gong, Y. Katsuyama, T. Kurokawa, Y. Osada, Double-network hydrogels with extremely high mechanical strength, Adv. Mater. 15 (14) (2003) 1155–1158, https://doi.org/10.1002/adma.200304907.
[40] Z.J. Wang, W. Li, X. Li, T. Nakajima, M. Rubinstein, J.P. Gong, Rapid self-strengthening in double-network hydrogels triggered by bond scission, Nat. Mater. 24 (2025) 607–614, https://doi.org/10.1038/s41563-025-02137-6.
[41] S. Li, F. Yang, K. Xiang, J. Chen, Y. Zhang, J. Wang, J. Sun, Y. Li, A Multifunctional Microspheric Soil Conditioner Based on Chitosan-Grafted Poly(acrylamide-co-acrylic acid)/Biochar, Langmuir 38 (18) (2022) 5717–5729, https://doi.org/10.1021/acs.langmuir.2c00317.
[42] S.R. Stauffer, N.A. Peppast, Poly(vinyl alcohol) hydrogels prepared by freezing-thawing cyclic processing, Polymer 33 (18) (1992) 3932–3936, https://doi.org/10.1016/0032-3861(92)90385-A.
[43] S. Narukulla, S. Bogadi, V. Tallapaneni, B.K.R. Sanapalli, S. Sanju, A.A. Khan, A. Malik, H.R. Barai, T.K. Mondal, V.V.S.R. Karri, A. Alexiou, S.K.S.S. Pindiprolu, G. Kuppusamy, V. Subramaniyan, M. Rabiul Islam, M. Papadakis, Comparative study between the Full Factorial, Box–Behnken, and Central Composite Designs in the optimization of metronidazole immediate release tablet, Microchem. J. 207 (2024) 111875, https://doi.org/10.1016/j.microc.2024.111875.
[44] Y. Leng, C.N. Britten, F. Tarannum, K. Foley, C. Billings, Y. Liu, K.B. Walters, Stimuli-Responsive Phosphate Hydrogel: A Study on Swelling Behavior, Mechanical Properties, and Application in Expansion Microscopy, ACS Omega 9 (36) (2024) 37687–37701, https://doi.org/10.1021/acsomega.4c02475.
[45] J. Zhang, K. Fu, D. Wang, S. Zhou, J. Luo, Refining hydrogel-based sorbent design for efficient toxic metal removal using machine learning-Bayesian optimization, J. Hazard. Mater. 479 (2024) 135688, https://doi.org/10.1016/j.jhazmat.2024.135688.
[46] R. Mohafezatkar Gohari, M. Safarnia, A. Dadvand Koohi, M. Baghban Salehi, Adsorptive removal of cationic dye by synthesized sustainable xanthan gum-g p (AMPS-co-AAm) hydrogel from aqueous media: Optimization by RSM-CCD model, Chem. Eng. Res. Des. 188 (2022) 714–728, https://doi.org/10.1016/j.cherd.2022.10.028.
[47] A. Nair, Y.K. Kumawat, S. Choudhary, J. Nath, K. Sharma, T. Rasool, V. Sharma, V. Kumar, Malachite green dye adsorption from wastewater using pine gum-based hydrogel: Kinetic and thermodynamic studies, J. Mol. Struct. 1295 (2024) 136671, https://doi.org/10.1016/j.molstruc.2023.136671.
[48] A.K. Sharma, B.S. Kaith, V. Tanwar, J.K. Bhatia, N. Sharma, S. Bajaj, S. Panchal, RSM-CCD optimized sodium alginate/gelatin based ZnS-nanocomposite hydrogel for the effective removal of biebrich scarlet and crystal violet dyes, Int. J. Biol. Macromol. 129 (2019) 214–226, https://doi.org/10.1016/j.ijbiomac.2019.02.034.
[49] F. Amalina, A. Syukor Abd Razak, S. Krishnan, H. Sulaiman, A.W. Zularisam, M. Nasrullah, Advanced techniques in the production of biochar from lignocellulosic biomass and environmental applications, Clean. Mater. 6 (2022) 100137, https://doi.org/10.1016/j.clema.2022.100137.
[50] Y. Liu, Y. Zhu, B. Mu, Y. Wang, Z. Quan, A. Wang, Synthesis, characterization, and swelling behaviors of sodium carboxymethyl cellulose-g-poly(acrylic acid)/semi-coke superabsorbent, Polym. Bull. 79 (2) (2022) 935–953, https://doi.org/10.1007/s00289-021-03545-9.
[51] S.-H. Kong, S.K. Loh, R.T. Bachmann, H. Zainal, K.Y. Cheong, Palm kernel shell biochar production, characteristics and carbon sequestration potential, J. Oil Palm. Res. 31 (3) (2019) 508–520, https://doi.org/10.21894/jopr.2019.0041.
[52] Y. Wu, C. Brickler, S. Li, G. Chen, Synthesis of microwave-mediated biochar-hydrogel composites for enhanced water absorbency and nitrogen release, Polym. Test. 93 (2021) 106996, https://doi.org/10.1016/j.polymertesting.2020.106996.
[53] S. Cui, F. Yang, D. Yu, C. Shi, D. Zhao, L. Chen, J. Chen, Double network physical crosslinked hydrogel for healing skin wounds: New formulation based on polysaccharides and Zn^{2+}, Int. J. Mol. Sci. 24 (17) (2023) 13042, https://doi.org/10.3390/ijms241713042.
[54] A. Shi, X. Dai, Z. Jing, Tough and self-healing chitosan/poly(acrylamide-co-acrylic acid) double network hydrogels, Polym. Sci. A. 62 (3) (2020) 228–239, https://doi.org/10.1134/S0965545X20030128.
[55] Q. Lv, Y. Shen, Y. Qiu, M. Wu, L. Wang, Poly(acrylic acid)/poly(acrylamide) hydrogel adsorbent for removing methylene blue, J. Appl. Polym. Sci. 137 (43) (2020) 49322, https://doi.org/10.1002/app.49322.
[56] S. Chen, L. Wu, Z. Wu, Z. Liu, Z. Qiu, L. Chi, Highly efficient removal of Sr^{2+} from aqueous solutions using a polyacrylic acid/crown-ether/graphene oxide hydrogel composite, RSC Adv. 14 (11) (2024) 7825–7835, https://doi.org/10.1039/D3RA08789A.
[57] M. Petousis, E. Maravelakis, D. Kalderis, V. Saltas, N. Mountakis, M. Spiridaki, N. Bolanakis, A. Argyros, V. Papadakis, N. Michailidis, Biochar for sustainable additive manufacturing: Thermal, mechanical, electrical, and rheological responses of polypropylene-biochar composites, Biomass Bioenergy 186 (2024) 107272, https://doi.org/10.1016/j.biombioe.2024.107272.
[58] S.E. Fang, R. Perera, Damage identification using response surface methodology, Key Eng. Mater. 413-414 (2009) 669–676, https://doi.org/10.4028/www.scientific.net/KEM.413-414.669.
[59] K.P. Sambasevam, S.F. Sateria, S.N.A. Baharin, N.J. Azman, S. Ahmad Wakid, S. Shahabuddin, An optimization of fungal chitin grafted polyaniline for ammonia gas detection via Box Behnken design, Int. J. Biol. Macromol. 238 (2023) 124079, https://doi.org/10.1016/j.ijbiomac.2023.124079.
[60] S. Dan, M. Kalantari, A. Kamyabi, M. Soltani, Synthesis of chitosan-g-itaconic acid hydrogel as an antibacterial drug carrier: optimization through RSM-CCD, Polym. Bull. 79 (10) (2022) 8575–8598, https://doi.org/10.1007/s00289-021-03903-7.

[61] S. Soleimani, A. Heydari, M. Fattahi, Swelling prediction of calcium alginate/cellulose nanocrystal hydrogels using response surface methodology and artificial neural network, Ind. Crops Prod. 192 (2023) 116094, https://doi.org/10.1016/j.indcrop.2022.116094.
[62] S. Heidari, M. Mohammadi, F. Esmaeilzadeh, D. Mowla, Determination of Swelling Behavior and Mechanical and Thermal Resistance of Acrylamide–Acrylic Acid Copolymers under High Pressures and Temperatures, ACS Omega 6 (37) (2021) 23862–23872, https://doi.org/10.1021/acsomega.1c02638.
[63] S. Bikbulatova, A. Tahmasebi, Z. Zhang, S.K. Rish, J. Yu, Understanding water retention behavior and mechanism in bio-char, Fuel Process. Technol. 169 (2018) 101–111, https://doi.org/10.1016/j.fuproc.2017.09.025.
[64] Y. Song, S. Zhang, J. Kang, J. Chen, Y. Cao, Water absorption dependence of the formation of poly(vinyl alcohol)-iodine complexes for poly(vinyl alcohol) films, RSC Adv. 11 (46) (2021) 28785–28796, https://doi.org/10.1039/D1RA04867H.
[65] F. Mo, L. Hang, M. Xu, L. Cheng, M. Cui, L. Chen, G. Liang, J. Wei, Rational design of dynamically super-tough and super-stretchable hydrogels for deformable energy storage devices, Small 20 (25) (2024) 2305557, https://doi.org/10.1002/smll.202305557.
[66] H.H.M. Rapaiee, D. Julaihi, M.I.A. Nordin, F.K. Liew, S.F. Sim, C.-K. Chiam, L.T. L. Than, C.Y. Lin, N.A. Tajuddin, S.S. Lam, L.-C. Wang, C.S.Y. Tan, Sodium humate-functionalised superabsorbent hydrogels for heavy metals and organic dyes remediation in aqueous systems, Inorg. Chem. Commun. 181 (2) (2025) 115326, https://doi.org/10.1016/j.inoche.2025.115326.
[67] X. Xu, V.V. Jerca, R. Hoogenboom, Bioinspired double network hydrogels: from covalent double network hydrogels via hybrid double network hydrogels to physical double network hydrogels, Mater. Horiz. 8 (4) (2021) 1173–1188, https://doi.org/10.1039/D0MH01514H.
[68] J. Ding, Y. Yang, J. Poisson, Y. He, H. Zhang, Y. Zhang, Y. Bao, S. Chen, Y.M. Chen, K. Zhang, Recent advances in biopolymer-based hydrogel electrolytes for flexible supercapacitors, ACS Energy Lett. 9 (4) (2024) 1803–1825, https://doi.org/10.1021/acsenergylett.3c02567.
[69] G. Iula, A. Raucci, L. Antonelli, P.M. Kalligosfyri, M.G. De Cesaris, N. Felli, C. Di Natale, S. Cinti, A. Gentili, Smart and sustainable 3D-printed electrochemical device for diclofenac remediation and monitoring in water, Talanta (2025) 128597, https://doi.org/10.1016/j.talanta.2025.128597.
[70] H. Adelnia, R. Ensandoost, S.S. Moonshi, J.N. Gavgani, E.I. Vasafi, H.T. Ta, Freeze/thawed polyvinyl alcohol hydrogels: Present, past and future, Eur. Polym. J. 164 (2022) 110974, https://doi.org/10.1016/j.eurpolymj.2021.110974.
[71] H. Jia, M. Xia, J. Li, H. Li, D. Chang, D. Yan, M. Lai, Y. Wei, P. Chang, X. Yang, X. Ji, Effect and mechanism of biochar-based hydrogel to alleviate drought stress in tobacco, Plant Stress 12 (2024) 100499, https://doi.org/10.1016/j.stress.2024.100499.
[72] A. El Idrissi, F. Tayi, O. Dardari, A. Akil, O. Amadine, L. Lu, M. Zahouily, Y. Essamlali, Development of multifunctional carboxymethyl starch-based semi-IPN hydrogels for water and fertilizer management in maize cultivation under different water deficit conditions, ACS Sustain. Chem. Eng. 13 (19) (2025) 7286–7298, https://doi.org/10.1021/acssuschemeng.5c02331.
[73] Z.F. Akl, E.G. Zaki, S.M. ElSaeed, Green hydrogel-biochar composite for enhanced adsorption of uranium, ACS Omega 6 (50) (2021) 34193–34205, https://doi.org/10.1021/acsomega.1c01559.
[74] S. Datta Chaudhuri, A. Mandal, A. Dey, D. Chakrabarty, Tuning the swelling and rheological attributes of bentonite clay modified starch grafted polyacrylic acid based hydrogel, Appl. Clay Sci. 185 (2020) 105405, https://doi.org/10.1016/j.clay.2019.105405.
[75] J. Li, Y. Zhu, M. Liu, Z. Liu, T. Zhou, Y. Liu, D. Cheng, Network interpenetrating slow-release nitrogen fertilizer based on carrageenan and urea: A new low-cost water and fertilizer regulation carrier, Int. J. Biol. Macromol. 242 (2023) 124858, https://doi.org/10.1016/j.ijbiomac.2023.124858.
[76] T.A. Adjuik, S.E. Nokes, M.D. Montross, Biodegradability of bio-based and synthetic hydrogels as sustainable soil amendments: A review, J. Appl. Polym. Sci. 140 (12) (2023) e53655, https://doi.org/10.1002/app.53655.
[77] C. Buchmann, J. Neff, M. Meyer, M. Bundschuh, Z. Steinmetz, Superabsorbent polymers in soil: The new microplastics? Camb. Prism. Plast. 2 (2024) e3 https://doi.org/10.1017/plc.2024.2.
[78] Z. Guo, Z. Wang, W. Pan, The preparation of PVA/PBS/LiCl hydrogels and their performance as conductive gels, Micro Nano Lett. 18 (9-12) (2023) e12181, https://doi.org/10.1049/mna2.12181.
[79] D. Wang, Y. Zheng, Q. Deng, X. Liu, Water-soluble synthetic polymers: their environmental emission relevant usage, transport and transformation, persistence, and toxicity, Environ. Sci. & Technol. 57 (16) (2023) 6387–6402, https://doi.org/10.1021/acs.est.2c09178.
[80] S. Ahmad, K. Manzoor, R. Purwar, S. Ikram, Morphological and swelling potential evaluation of *Moringa oleifera* gum/poly(vinyl alcohol) hydrogels as a superabsorbent, ACS Omega 5 (29) (2020) 17955–17961, https://doi.org/10.1021/acsomega.0c01023.
[81] S.-J. Jong, S.-F. Chin, M.E. Wasli, Cellulose based hydrogel as soil conditioner and seed germination medium, Sci. Rep. 15 (1) (2025) 22648, https://doi.org/10.1038/s41598-025-05920-2.
[82] A.A. Abdelgelil, A.M. Omer, A.F. Hassan, A.A. Moustafa, M.S. Mohy Eldin, Enhancement of sandy soil water retention using superabsorbent carboxymethyl cellulose grafted with polyacrylamide and polyacrylamidomethyl propanesulfonic acid copolymer, Sci. Rep. 15 (1) (2025) 16604, https://doi.org/10.1038/s41598-025-94490-4.
[83] Z. Gao, F. Du, G. Fu, X. Yang, Y. Wei, M. Lai, D. Chang, X. Ji, Effect of a sodium carboxymethyl cellulose composite hydrogel on tobacco growth and development under drought stress, Int. J. Biol. Macromol. 309 (2025) 142700, https://doi.org/10.1016/j.ijbiomac.2025.142700.
[84] S. Fang, G. Wang, R. Xing, X. Chen, S. Liu, Y. Qin, K. Li, X. Wang, R. Li, P. Li, Synthesis of superabsorbent polymers based on chitosan derivative graft acrylic acid-co-acrylamide and its property testing, Int. J. Biol. Macromol. 132 (2019) 575–584, https://doi.org/10.1016/j.ijbiomac.2019.03.176.
[85] A. Olad, F. Doustdar, H. Gharekhani, Starch-based semi-IPN hydrogel nanocomposite integrated with clinoptilolite: Preparation and swelling kinetic study, Carbohydr. Polym. 200 (2018) 516–528, https://doi.org/10.1016/j.carbpol.2018.08.014.
[86] M.D. Bucevschi, Z. Meiri, S. Shahal, Polymeric composition for use as soil conditioner with improved water absorbency during watering of the agricultural crops, U.S. Patent No. 12,129,419, Polygreen Ltd, 29 October 2024.
[87] K. Rahimi Mamaghani, M. Alikarami, H. Saremi, Polymeric Hydrogels in Agriculture: Environmental Performance, Sustainability Challenges, and Future Perspectives, ACS Agric. Sci. & Technol. 5 (12) (2025) 2341–2360, https://doi.org/10.1021/acsagscitech.5c00808.
[88] J. Li, L. Li, Y. Zhang, Q. Zhang, Y. Wang, X. Yu, Bio-based hydrogel particles with enhanced water retention properties for alleviating drought stress of saline soil, J. Clean. Prod. 518 (2025) 145960, https://doi.org/10.1016/j.jclepro.2025.145960.
[89] Z. Steinmetz, C. Plicht, C. Buchmann, M. Knott, M. Meyer, S. Mueller-Schuessele, D. Strieth, M.H. Prosenc, H. Steinmetz, H.F. Jungkunst, Plastic problem solved? Environmental implications of synthetic hydrophilic polymers across ecosystem boundaries, TrAC Trends Anal. Chem. 181 (2024) 118000, https://doi.org/10.1016/j.trac.2024.118000.